8-8-2019

Combining Hyperspectral Imaging and Small Unmanned Aerial Systems for Grapevine Moisture Stress Assessment

Rinaldo R. Izzo
rri2143@rit.edu

Combining Hyperspectral Imaging and Small Unmanned Aerial Systems for Grapevine Moisture Stress Assessment

by

Rinaldo R. Izzo

B.S. Worcester Polytechnic Institute, 2013
M.B.A. University of California, Los Angeles 2017

A thesis submitted in partial fulfillment of the
requirements for the degree of Master of Science
in the Chester F. Carlson Center for Imaging Science
College of Science
Rochester Institute of Technology

August 8, 2019

Signature of the Author _____

Accepted by _____

Coordinator, M.S Degree Program Date

CHESTER F. CARLSON CENTER FOR IMAGING
SCIENCE COLLEGE OF SCIENCE
ROCHESTER INSTITUTE OF TECHNOLOGY
ROCHESTER, NEW YORK

CERTIFICATE OF APPROVAL

M.S. DEGREE THESIS

The M.S. Degree Thesis of Rinaldo R. Izzo
has been examined and approved by the
thesis committee as satisfactory for the
thesis required for the
M.S. degree in Imaging Science

Dr. Jan van Aardt
Thesis Advisor

Dr. Carl Salvaggio
Committee Member

Dr. Emmett Ientilucci
Committee Member

Date

Combining Hyperspectral Imaging and Small Unmanned Aerial Systems for Grapevine Moisture Stress Assessment

by

Rinaldo R. Izzo

Submitted to the
Chester F. Carlson Center for Imaging Science
in partial fulfillment of the requirements
for the Master of Science Degree
at the Rochester Institute of Technology

Abstract

It has been shown that mild water deficit in grapevine contributes to wine quality, in terms of especially grape and subsequent wine flavor. Water deficit irrigation and selective harvesting are implemented to optimize quality, but these approaches require rigorous measurement of vine water status. While traditional in-field physiological measurements have made operational implementation onerous, modern small unmanned aerial systems (sUAS) have presented the unique opportunity for rigorous management across vast areas. This study sought to fuse hyperspectral remote sensing, sUAS, and sound multivariate analysis techniques for the purposes of assessing grapevine water status. High-spatial and -spectral resolution hyperspectral data were collected in the visible/near-infrared (VNIR; 400-1000nm) and short-wave infrared (SWIR; 950-2500 nm) spectral regions across three flight days at a commercial vineyard in the Finger Lakes region of upstate New York. A pressure chamber was used to collect traditional field measurements of stem water potential (ψ_{stem}) during image acquisition. We completed some preliminary exploration of spectral smoothing, signal-to-noise ratio, and calibration techniques in forging our experimental design. We then correlated our hyperspectral data with a limited stress range (wet growing season) of traditional measurements for ψ_{stem} using multiple linear regression (R^2 between 0.34 and 0.55) and partial least squares regression (R^2 between 0.36 and 0.39). We demonstrated statistically significant trends in our experiment, further qualifying the potential of hyperspectral data, collected via sUAS, for the purposes of grapevine water management. There was indication that the chlorophyll and carotenoid absorption regions in the VNIR, as well as

several SWIR water band regions warrant further exploration. This work was limited since we did not have access to experimentally-controlled plots, and future work should ensure a full range of water stress. Ultimately, models will need validation in different vineyards with a full range of plant stress.

Acknowledgments

I would like to thank all those individuals who never stopped believing in me throughout my life, through good times and bad times. I am forever grateful to those who continuously have pushed me to be a better version of myself each new day.

Disclaimer Clause

The views expressed in this thesis are those of the author and do not reflect the official policy or position of the United States Air Force, Department of Defense, or the U.S. Government.

Contents

List of Figures

List of Tables

Chapter 1

Introduction

1.1 CONTEXT

Grapes arguably are one of the most economically-important agricultural crops in the world; in 2007, vineyards comprised 7.8 million hectares around the world, with a yield of around 65 million metric tons, per figures from Bayer Crop Science (Bayer 2019). While somewhat constrained to the more temperate geographic zones around the world, vineyards indeed stretch across the globe to include presence in countries like Spain, France, Italy, Turkey, China, USA, etc. If the specific geologic conditions coincide, vineyards can be found even in less than ideal locations, such as the Finger Lakes region of Upstate New York, USA. While much of the cultivated grape crop is dedicated for food or table grape purposes, the vast majority of cultivated grapes are destined for manufactured wine products. It is estimated that around 270 million hectoliters of wine products were produced worldwide in 2007 (Bayer 2019). Thus, it can be presumed that there is a significant interest in maintaining and increasing the associated quality of wine product for economic and cultural reasons.

The eventual quality, taste, and style of wine products are highly influenced by *terroir*, a nod to the environmental, geographic, and human conditions under which grapevines are grown

and cultivated (Cornelis Van Leeuwen and Seguin 2006). Contrary to common convention with most agricultural crops, grapevine and associated harvest quality actually benefit from suboptimal ecological settings, especially in terms of mild moisture deficits, which has been shown to in fact aid the quality of cultivated grapes for wine. The presence of a mild moisture deficit in grapevines prompts a reduction in shoot growth, berry weight, and yield, all of which are factors that collectively serve to inflate berry anthocyanin and tannin levels and, as such, perceived quality (Cornelis Van Leeuwen et al. 2009). The idea of leveraging mild moisture deficit for quality potential is especially prevalent in red wine. With the opportunity to regulate quality, given moisture condition, comes the challenge to properly control water deficit in the vines, since severe deficit can be detrimental to yield and quality (Ojeda et al. 2002).

Controlled deficit irrigation therefore has emerged as one method to induce mild moisture deficit stress in grapevines, and has been demonstrated to yield improved berry quality, while maintaining operationally acceptable yields (Chaves et al. 2007). Deficit irrigation, or partial irrigation, reduces vine vigour and shoot growth in a controlled manner that shifts plant metabolic processes to induce improved fruit quality (Matthews and Anderson 1989). Similarly, in vineyards where deficit irrigation techniques cannot be realized, the knowledge of vine water status may dictate selective harvesting practices, giving way to optimized quality and yield. Selective harvesting can be successfully implemented in both small quantity producing wineries, as well as those with large volume and flexible infrastructure (Bramley et al. 2005). It subsequently stands to reason that a scheme to control grapevine moisture inevitably demands accurate and rigorous measurements of grapevine moisture at any given time.

Traditionally, management of vine moisture status has been facilitated by direct in-field measurement of sensitive physiological indicators. Stem water potential (ψ_{stem}), a measure of integral plant transpiration and an indicator of the capability for grapevines to conduct water from the soil to the atmosphere, has been validated as one such sensitive indicator that may aid vine moisture management (Chone et al. 2001). A pressure chamber typically is used to measure the negative pressure in the xylem of plants in order to gauge the underlying ψ_{stem} associated with a given vine (Scholander et al. 1965). The in-field direct measurement of ψ_{stem} with a manual pressure chamber, while proven valid for grapevine water status measurement (Chone et al. 2001), is challenging for large, commercial vineyards. While strides have been made in numerous vineyard settings to operationally respond to in-field measures of vine moisture status, accurate

measurements often require an inordinate amount of time and labor, and progress in operational application remains gradual (Rodríguez-Pérez et al. 2007).

It is in this context that remote sensing technology has become an increasingly common tool to remotely probe for plant physiological indicators, like plant moisture status, via observations of the unique electromagnetic spectral response related to plant moisture regimes. The potential superiority of non-destructive remote sensing techniques, for these purposes, lies in the cost-effective, exhaustive ("wall-to-wall"), and objective nature of application (Govender et al. 2009). Significant progress in the spectral and spatial granularity of enabling sensors has made the operational implementation of such sensors for precision field application more tenable. As such, many recent works have assessed remote sensing as a more realistic operational tool that could allow larger-scale decision making by vineyard managers (De Bei et al. 2011; Acevedo-Opazo et al. 2008; Jones et al. 2009).

Hyperspectral data collected via remote sensing techniques can be particularly useful when trying to ascertain underlying plant physiology, mainly due to the data type's fine spectral granularity. In the visible (VIS) regime of the spectrum, i.e., 400-700 nanometers (nm), and the near-infrared (NIR) regime, 700-1000 nm, subtle variations in photosynthetic pigments, such as chlorophyll and carotenoids, and leaf structure variations are evident (Josep Peñuelas and Filella 1998). In the shortwave infrared (SWIR) regime, i.e., 1000-2500 nm, several strong atmospheric absorption bands are present and vegetation moisture content dominates as the primary influence of plant spectral signatures (Behmann, Steinrücken, and Plümer 2014). Hyperspectral signatures of vegetation thus allow insight into specific spectral characteristics or indicators, which might be useful as proxies for key physiology states. However, with the very fine spectral nature of hyperspectral data, there is a need to apply sound modeling techniques to reduce data dimensionality, remove the noise associated with highly correlated variables, and identify wavelengths of greatest importance (Thenkabail, Lyon, and Huete 2011).

It then becomes a question as to how exactly to collect, process, and analyze remote sensing data for use in plant physiological studies. Field spectroradiometers often are used in studies to enable relatively fast and simple data collection; however, spectroradiometers limit the operational utility for large area applications and arguably represent best-case, low-noise scenarios and results still require scaling to operational image resolutions and extents. The application of aircraft or

satellite platforms as the modalities via which to collect plant spectral data at a precise level remains inhibitive, on the other hand, mainly due to shortcomings in spatial and temporal resolutions, as well as strict adherence to weather conditions. It is in this context that small unmanned aerial systems (sUAS) platform for precision agriculture application arguably balances the demands for low cost, high spatial/spectral/temporal resolutions, and ease of use, and lends itself well to moisture management applications (Gago et al. 2015). We therefore attempted to further explore the utility of high-spectral, high-spatial resolution sUAS-collected data for grapevine moisture management.

Our research fused hyperspectral remote sensing, sUAS, and sound multivariate analysis techniques for the purposes of assessing grapevine water status. We conducted full airborne (sUAS) and ground (field truth) campaigns and analyzed our data using sound modeling techniques, all in order to present trends and conclusions to inform future efforts. The targeted objectives for the research are presented in the subsequent section.

1.2 OBJECTIVES

Our overarching objective was to assess the utility of sUAS-based (hyper-) spectral indicators for assessing limited variation in vineyard moisture status, toward establishing potential operational solutions. Our specific objectives were as follow:

- Objective 1: Evaluate a sound data processing chain to relate hyperspectral data and field (moisture) physiological indicators for a commercial, rainfed vineyard.
- Objective 2: Assess the overall potential of sUAS-based hyperspectral remote sensing for managing grapevine moisture status.
- Objective 3: Identify pertinent spectral indicators in the VNIR spectral regime for discerning grapevine moisture status.
- Objective 4: Identify pertinent spectral indicators in the SWIR spectral regime for discerning grapevine moisture status.

The research findings from these objectives were reported as a conference proceedings paper and comprehensive technical manuscript for targeted outreach.

1.3 THESIS LAYOUT

1.3.1 Chapter 2: Background

This chapter provides a brief review of some of the seminal work done in relation to remote sensing for grapevine moisture assessment. It provides a more comprehensive background to set up and further motivate Chapters 3 and 4, the core research chapters.

1.3.2 Chapter 3: A cursory analysis of real-time sUAS-based detection of grapevine water status in the Finger Lakes Wine Country of Upstate New York

This chapter represents a paper that was presented and published in the Autonomous Air and Ground Sensing Systems for Agricultural Optimization and Phenotyping session of the SPIE Defense and Commercial Sensing Conference proceedings, April 2019 (Izzo et al. 2019). It details initial modeling and data analysis efforts for the VNIR data that we had collected at Fox Run Vineyards in Upstate New York, USA. This paper addresses Objectives 1, 2, and 3.

1.3.3 Chapter 4: Combining hyperspectral imaging and small unmanned aerial systems for grapevine moisture stress assessment

This chapter further expands upon the results of Chapter 3 by including the sUAS SWIR imagery and three days' worth of field to better discern links to plant physiological phenomena. This chapter is written with the intent to publish in an applicable journal in the 2019 timeframe and addresses Objectives 2, 3, 4, and 5.

1.3.3 Chapter 5: Summary

This chapter provides a summary of the work and suggested improvements for future related research.

1.4 SCIENTIFIC CONTRIBUTIONS

This research is by no means the first remote sensing study related to vineyard moisture assessment, with previous efforts focusing mostly on in situ spectroradiometers and multispectral sUAS platforms. However, our effort does represent cutting-edge work in fine-scale (high spatial resolution) hyperspectral imagery, across the full reflective domain (400-2500 nm). Specifically, we:

- demonstrated sound data processing chain to relate hyperspectral data and field physiological indicators for a commercial rainfed vineyard, absent access to experimental field plots, including pixel classification and multivariate modeling techniques;
- proved that correlation can be established between field ψ_{stem} and hyperspectral data of grapevine, even given a relatively narrow-range of ψ_{stem} response; and
- showed statistically-significant trends when relating grapevine ψ_{stem} to downsampled hyperspectral data collected across the VNIR and SWIR spectral regimes (400-2500 nm)
    - in the VIS, we suggested the importance of understanding the chlorophyll and carotenoid absorption regions for grapevine,
    - in the NIR, we confirmed the minor water absorption feature (970 nm) a useful indicator for understanding grapevine moisture, as already indicated by a number of established spectral indices in the literature, and
    - in the SWIR, we pointed to select longer wavelength regions that might be considered in grapevine moisture studies

These contributions were presented and published in part in the Autonomous Air and Ground Sensing Systems for Agricultural Optimization and Phenotyping session of the SPIE Defense and Commercial Sensing Conference proceedings, April 2019 (Izzo et al. 2019) (Chapter 3), while we also intend to publish a journal article in the 2019 timeframe as a more comprehensive reporting of the work (Chapter 4).

Chapter 2

Background

2.1 FOREWORD

This thesis is organized in a modern format, such that the primary chapters (Chapter 3 and Chapter 4) each represent past or intended publications. This chapter provides a brief literature review and background to further set up the primary Chapters 3 and 4. Chapter 2 therefore provides a review of previous related work in remote sensing of grapevine water across a number of data collection platforms and modeling techniques.

2.2 PASSIVE REMOTE SENSING

The major body of previous research in remote sensing studies of grapevine moisture, including the work presented in this thesis, is predicated on passive remote sensing. As such, this section seeks to provide a review of passive remote sensing studies completed in the optical and thermal sensing regimes.

2.2.1 Optical remote sensing

Image and point-based spectral data can be collected in the visible (400-700 nm) and infrared spectral regimes (700-2500 nm) with optical remote sensing. The captured solar radiation reflected off of targets can provide an indication of the composition of such targets (Hall et al. 2002). For example, vegetation has a known reflectance spectrum that can be interrogated, but even further, species and physiology can be ascertained from the detail of that spectral signal (Josep Peñuelas and Filella 1998). It should be noted that sensing in the visible regime typically is more affordable, practical, and even operational in experimental design, when compared to the infrared spectral regions, mainly due to material limitations in detectors. The utility of spectral signatures is often dependent upon the spectral resolution of the sensor used for data collection; specifically, multispectral imaging systems capture just a few broad bands, while hyperspectral sensors capture many (often hundreds) of narrow, contiguous bands. In the past remote sensing studies of grapevine moisture, while some of the work has tried to use multispectral technology, most implemented hyperspectral technology with fine spectral detail, but using in situ sensing approaches (Govender et al. 2009).

Many previous studies have explored existing spectral indices to better understand the utility of these universal indices for ore specific applications. For example, Rodríguez-Pérez et al. (2007) related hyperspectral reflectance data (350-2500 nm), collected in a commercial vineyard of Pinot noir and using an integrating sphere and field spectroradiometer, to numerous known reflectance indices. They evaluated the difference between midday ψ_{stem} and pre-dawn leaf water potential, and achieved strong fits with the Red/Green Index (R^2 = 0.619) and the structure intensive pigment index (R^2 = 0.541). Serrano et al. (2012) used a spectroradiometer covering 400-1100 nm to capture spectral data of leaves in a rainfed vineyard across 256 spectral channels. They aimed to investigate the relation between the normalized difference vegetation index (NDVI) and berry yield/composition during mild to moderate moisture stress conditions. They found NDVI to model total soluble solids (R^2 = 0.81) and maturity index at harvest (R^2 = 0.89) reasonably well, while the Water Index performed well with regards to titratable acidity (R^2 = 0.62) and the maturity index (R^2 = 0.67).

Other researchers have proposed novel indices, which might prove useful in understanding grapevine moisture status, thereby recognizing the risk in applying universal spectral indices for

specific applications. Maimaitiyiming et al. (2017) worked in an experimental vineyard to apply different irrigation treatments to better understand grapevine moisture stress; the authors performed an exhaustive search of normalized difference spectral indices (NDSI) to propose those with strongest relationships to water proxies. They found that stomatal conductance was the best proxy for underlying water stress and that the wavelengths at 603 and 558 nm should be used in an normalized difference spectral index (NDSI). Rapaport et al. (2015) correlated visible and shortwave infrared data, collected with ground spectrometers, to midday leaf water potential, stomatal conductance, and non-photochemical quenching using partial least squares regression. Recognizing significant reflectance trends in the regions of 530-550 nm and near 1500 nm, they proposed three novel normalized water balance indices (WABI) utilizing these regions.

Others still have explored whether retaining all data in spectral signatures, rather than downselecting to indices, would be beneficial in grapevine moisture studies. For example, Loggenberg et al. (2018) meshed machine learning techniques – random forest (RF) and extreme gradient boosting – and hyperspectral data with the aim to classify stressed versus non-stressed Shiraz grapevine. They found that using a subset, i.e., 18 of 176 wavelength bands collected, in fact aided with slightly better classification accuracy (1.7% to 5.5 %). Rather than using spectral indices, Zovko et al. (2019) applied partial least squares analysis techniques to classify four water treatments of grapevine in a Croatian experimental vineyard, and pointed to pertinent spectral indicators. They specifically found that the O–H, C–H, and N–H stretches in water, carbohydrates, and proteins were of most pertinence in separating the water treatments.

2.2.1 Thermal remote sensing

In thermal remote sensing, or thermography, naturally emitted thermal radiation, usually in the regions of 3-5 μm and 8-14 μm, is captured to provide an indication of a target's temperature variation. Infrared thermography for instance can be used to interrogate the relationship between leaf stomatal closure and surface temperature (Jones et al. 2002). Since stomatal closure acts as a proxy for water activity in the plant, thermal imaging data can be useful in relating to plant physiological indicators. Recognizing this utility, we have seen a number of recent studies on grapevine moisture include thermal imaging as a means to relate to underlying physiological

indicators of grapevine moisture.

Möller et al. (2006) explored the use of thermal imaging to investigate water stress conditions in a northern Israel vineyard of Merlot by applying various irrigation levels. Using a FLIR thermal imaging system, they were able to correlate physiological indicators – including stem water potential, leaf conductance, and leaf area index – with the Crop Water Stress Index (CWSI). The CWSI, which compares canopy temperatures and meteorological conditions, was found to be significantly correlated with leaf conductance and stem water potential. The most significant R^2 metric was found in relating the CWSI to stomatal conductance ($R^2 = 0.91$). Pou et al. (2014) set out to validate thermal indices that had been previously associated with water status in grapevine, including the stomatal conductance index (I_g) and the CWSI. They found both of the aforementioned indices to be highly representative of stomatal conductance, with best results obtained when data were collected on the shaded portion of the canopy during midday. Finally, Fuentes et al. (2012) worked towards automating thermography for discerning water stress in grapevines. Significant correlations were proven between canopy temperature indices and traditional field physiological indicators, and a more fully automated technique was proposed by using ancillary weather data. The advent of unmanned aerial systems (UAS), however, has led to studies exploring this novel platform for more operational application scenarios.

2.3 UAS DATA COLLECTION PLATFORMS

The use of aircraft or satellites to probe plant water status is limiting, due to a dependence on ideal atmospheric conditions, lack of high enough spatial/spectral/temporal resolutions, and cost; however, the growing accessibility of sUAS has made plant-level physiological observations over large areas more pragmatic. sUAS platforms serve to connect field-level assessment with leaf-level observations in precision agriculture applications, where the response to plant physiology is often better understood at finer scales (Gago et al. 2015). The use of sUAS as a data collection platform in remote sensing thus allows for high spatial and temporal resolution, while remaining reasonable option for operational implementation on a larger spatial scale.

The benefits of sUAS have come to the fore and sUAS have been used in some recent works, even though the specific application of the sUAS platform is still emerging in grapevine

moisture studies. Primicerio et al. (2012) built a sUAS platform for site-specific vineyard management at an experimental vineyard in central Italy, collecting 63 multispectral images in total. Their results included vigour maps that clearly delineated crop heterogeneity and matched their field data (ground truth). Baluja et al. (2012) collected multispectral (six bands at 530, 550, 570, 670, 700 and 800 nm) and thermal imagery via sUAS to study water status variability in a commercial rainfed vineyard. The authors reported that the normalized difference vegetation index (NDVI) and TCARI/OSAVI (a ratio between chlorophyll absorption and a soil-adjusted index) exhibited the best correlation with ψ_{stem}, with $R^2 = 0.68$ and $R^2 = 0.84$, respectively. Zarco-Tejada et al. (2013), on the other hand, examined the Photochemical Reflectance Index (PRI) as a proxy for water stress condition in grapevine. Their data consisted of multispectral and thermal imagery captured during four airborne collection efforts. The authors presented a novel normalized PRI, taking into consideration canopy structure and chlorophyll content. Santesteban et al. (2017) more recently used a sUAS platform to assess water status variations within a vineyard, but implemented high-resolution (0.09 m) thermal images for a 7.5 ha vineyard; they found the crop water stress index (CWSI) to be well correlated with stem water potential and stomatal conductance.

We used two separate platforms to accommodate two separate sensor suites and their supporting hardware for the research presented in this thesis; see Figure 2.1. The DJI Matrice 600 multi-copter sUAS platform was selected as the base airframe for our flight campaigns due to its modular efficiency (https://www.dji.com/). Trimble Applanix-15 boards were implemented in the designs to further boast the direct georeferencing and inertial intelligence of the sUAS platforms (https://www.applanix.com/). Both flight sensor suites, one intended to encompass the VIS and NIR (VNIR) spectral regimes and the other the SWIR regime, were furnished by Headwall Photonics (http://www.headwallphotonics.com/). A Headwall Nano-Hyperspec® Hyperspectral Imaging Sensor, comprising 270 narrow bandwidth spectral bands from 400-1000 nanometers (nm), 640 spatial bands, and a 7.4 micrometer pixel width, covered the VNIR regime. Likewise, for the SWIR regime, the Headwall Micro-Hyperspec SWIR® extended spectral reach from 950-2500 nm with 170 narrow bandwidth spectral bands. UgCS ground station software was used for mission planning to achieve the required altitude and speed parameters for the sUAS platforms (https://www.ugcs.com/). More detailed information regarding our air and ground campaigns can be found in the primary, i.e., Chapters 3 and 4.

Figure 2.1. Two separate multi-copter platforms were employed in our air campaign efforts. Both multi-copter designs exploited the modular DJI Matrice 600 flying platform. One of the multi-copters was equipped with a VNIR imaging sensor, while the other was equipped with a SWIR imaging sensor; both sensors boasted high spectral resolution – hyperspectral – sensors provided by Headwall Photonics

2.4 RESEARCH GAP

There still is a need to further evaluate sUAS-based, high spatial resolution, and especially hyperspectral imagery for different geographic regions, thereby validating past efforts for different regions and grape varieties. Most of the prior work utilizes data that were collected in situ via spectroradiometers. For those studies that did include a sUAS platform, many did not evaluate the optical domain and some did not correlate with reliable physiological indicators. We therefore attempted to bridge that gap to some extent in this work, fusing hyperspectral remote sensing, sUAS, and sound multivariate analysis techniques for the purposes of assessing grapevine water status.

Chapter 3

A cursory analysis of real-time sUAS-based detection of grapevine water status in the Finger Lakes Wine Country of Upstate New York

3.1 FOREWORD

This chapter represents a paper that was presented and published in the Autonomous Air and Ground Sensing Systems for Agricultural Optimization and Phenotyping session of the SPIE Defense and Commercial Sensing Conference proceedings, April 2019 (Izzo et al. 2019). It details initial modeling and data analysis efforts for the VNIR data that we had collected at Fox Run Vineyards in Upstate New York. This paper addresses Objectives 1, 2, and 3.

3.2 ABSTRACT

The quality of grapes in the production of wine is highly influenced by vine water status, where optimal water deficit or selective harvesting can improve berry quality. It is in this context

that the rapid advancement in small unmanned aerial system (sUAS) technology and the potential application of real-time, high-spatial resolution hyperspectral imagery for vineyard moisture assessment, have become tractable. This study sought to further sUAS hyperspectral imagery as a tool to model water status in a commercial vineyard in Upstate New York. High-spatial resolution (2.5 cm ground sample distance) hyperspectral data were collected in the visible/near-infrared (VNIR; 400-1000nm) regime on three flight days. A Scholander pressure chamber was used to directly measure the midday stem water potential (ψ_{stem}) within imaged vines at the time of flight. High spatial resolution pixels enabled the targeting of pure (sunlit) vine canopy with vertically trained shoots and significant shadowing. We used the partial least squares-regression (PLS-R) modeling method to correlate our hyperspectral imagery with measured field water status and applied a wavelength band selection scheme to detect important wavelengths. We evaluated spectral smoothing and band reduction approaches, given signal-to-noise ratio (SNR) concerns. Our regression results indicated that unsmoothed curves, with the range of wavelength bands from 450-1000 nm, provided the highest model performance with $R^2 = 0.68$ for cross-validation. Future work will include hyperspectral flight data in the short-wave infrared (SWIR; 1000-2500 nm) regime that were also collected. Ultimately, models will need validation in different vineyards with a full range of plant stress.

3.3 INTRODUCTION

Remote sensing has become a widely adopted tool for informing the decisions of farmers and has served to further evolve the operational sphere of precision agriculture applications. Precision agriculture is recognized as the application of the right management practice, at the right place, and at the right time (Mulla 2013). However, remote sensing techniques were not always widely recognized for their potential commercial application in agriculture. As recently as the year 2000, remote sensing was regarded as nothing more than a research tool in agriculture, seldom implemented at the operational level (Bastiaanssen, Molden, and Makin 2000). Today, however, the recent technical advancements in enabling sensors, coupled with the growing associations between scientists and farmers, have created the opportunity for remote sensing to significantly change the landscape of modern agricultural management.

The relation between remote sensing spectral data and plant water response has been

broadly accepted as a worthwhile pursuit by both the remote sensing and agricultural communities. The mechanism of evapotranspiration, or the combined transpiration and evaporation of plant water throughout the life of a plant, can be inspected via the plant's electromagnetic or spectral response (Damm et al. 2018). Spectral data, collected via remote sensing platforms, have been utilized for numerous works exploring plant water physiological response (Ač et al. 2015; Buitrago et al. 2016; Maimaitiyiming et al. 2017; Ballester et al. 2018). The advantages in using remote sensing technologies for remotely probing plant moisture status may include cost effectiveness, synoptic coverage, increased economic productivity, and objective physiological assessment (Govender et al. 2009).

Grapevine has emerged as a sensible genus in which to exploit remote sensing technology for the purposes of precisely managing plant water status. Vine water conditions must be properly understood and ideally regulated, since the key factors affecting grape quality potential - climate, soil, and grapevine and their interactions known as "terroir" - are intimately related to the underlying vine water status (Cornelis Van Leeuwen and Seguin 2006). In vineyards where irrigation application can be regulated, the application of controlled deficit irrigation, or mild water stress condition, has been shown to provide economically sufficient yield, while improving berry and wine quality (Chaves et al. 2007). Even in vineyards where irrigation is not controlled, but rather environment alone dictates vine water uptake, the knowledge of vine water status could stimulate selective harvesting practices to optimize eventual quality and yield of end product (Bramley et al. 2005). The in-field direct measurement of stem water potential (ψ_{stem}) with a manual pressure chamber, while proven valid for grapevine water status measurement (Chone et al. 2001), is difficult for large, commercial vineyards. As a result, remote sensing has been gauged extensively by the scientific and agricultural communities as a more realistic operational tool that could allow larger-scale decision making by vineyard managers (De Bei et al. 2011; Acevedo-Opazo et al. 2008; Jones et al. 2009).

The use of aircraft or satellites to remotely probe plant water status, however, is severely limiting due to the inherent low resolution and infrequent sampling of a dynamic situation. The growing accessibility of small unmanned aerial systems (sUAS), on the other hand, has made plant-level physiological observations over large areas more pragmatic. The sUAS platform serves to connect field-level assessment with leaf-level observations in precision agriculture applications,

where the response to plant physiology is often better understood at finer scales (Gago et al. 2015). The sUAS has been the platform of choice for a myriad of recent remote sensing studies examining grapevine water status (Bellvert et al. 2014; Baluja et al. 2012; D. Turner, Lucieer, and Watson 2011).

While the sensors utilized for remote sensing studies observing grapevine water status have varied, hyperspectral sensors have emerged as a particularly effective choice due to the fine spectral granularity offered. The many hundreds of spectral bands associated with hyperspectral sensors offer a glimpse into subtle plant response that simply may be missed with a coarser, more limited multispectral sensor. Recent works also have highlighted the utility of hyperspectral sensors for studying grapevine water status (Rapaport et al. 2015). It is in this context that our ongoing effort, presented in part in this manuscript, examines the potency of using hyperspectral data, collected via sUAS platform, for the purposes of accurately estimating real-time water status in grapevines. While many previous studies have examined the use of sUAS or hyperspectral sensing for observing grapevine water status, there remains a gap related to the combination of sUAS platforms and hyperspectral sensors for these purposes.

3.4 METHODOLOGY

3.4.1 Study area

The field work for this study was completed at a single mature commercial vineyard in the Finger Lakes Wine Country of Upstate New York, namely Fox Run Vineyards. The Finger Lakes premium wine region has grown significantly over the last few decades, boasting more than 11,000 acres of planted vineyards across more than 100 wineries, spread across Upstate New York in 2017 (“Finger Lakes Wine” 2017). This region is a glaciated lake region with cold winters and moderate, humid summer and variable rainfall. Fox Run, with grapes first planted in 1984, sits upon the western edge of Seneca Lake, New York, USA. The vineyard grows five different grape varietals—Riesling, Chardonnay, Lemberger, Cabernet Franc, and Cabernet Sauvignon—and produced around 18,000 cases in 2018 (“History of Fox Run” 2019).

Fox Run Vineyards is somewhat unique relative to many vineyards, due to its specific geological features. A significant portion of the property stands atop a thick layer of fertile, well-

drained sandy loam, left behind due to the receding shoreline of Seneca Lake over time. Gravelly silty loam dominates much of the rest of the vineyard, leaving behind evidence of a paleodelta formed after glacial melting ("Geological Features of Fox Run Vineyards in the Finger Lakes" 2019). Fox Run offers a complex terroir that provides a natural range of stress for environmental and scientific studies. A detailed vineyard map of Fox Run Vineyards is provided in Appendix A ("Vineyard Map of Fox Run Vineyards" 2019).

3.4.2 Data collection

This study consisted of both an air and ground campaign, to collect flight data to be properly correlated with in-field physiological measurements, taken at the time of flight, with more traditional measurement methods. Air and ground data, used to support the study, were collected on three sunny days during the 2018 growing season: 21 June, 15 August, and 17 September.

The Rochester Institute of Technology (RIT) has developed an UAS research laboratory and provided access to two sUAS platforms for our airborne campaign. Both platforms support sensor suites on DJI Matrice 600 multi-copters, pictured in Figure 3.1 below, with inertial sensory information fed through a Trimble Applanix-15 board (DJI 2019; Trimble Navigation 2017). The spectral sensors aboard both multi-copters were provided by Headwall Photonics; the sensor suite on one of the platforms covered the visible-near infrared (VNIR) spectral regime, while the other covered the shortwave infrared (SWIR) spectral regime. It should be noted that the initial results provided in this manuscript focus only on the VNIR regime flights.

The Headwall Nano-Hyperspec® Hyperspectral Imaging Sensor was selected for use on our VNIR platform. The wavelength range for the Nano-Hyperspec® extends from 400-1000 nm, consisting of 270 narrow spectral bands. The sensor uses CMOS camera technology, with 12-bit depth, 350 Hertz maximum frame rate, and detector with 7.4 micrometer pixel width (Headwall 2018).

UgCS ground station software facilitated the optimization of flight altitude and platform speed, based upon the desired ground sample distance (GSD; 2.5 cm in our case) (SPH 2019). It should be noted that there will be some level of image blur (platform motion) and effects due to the optical system's point spread function. Consideration of these two effects becomes especially important when selecting an even finer spatial resolution during flights. A high spatial resolution (GSD), e.g., 1 cm, would require increased integration times to maintain the signal-to-noise ratio

and could lead to notable image degradation due to increased blur, if platform velocity is not adapted accordingly (Tico and Vehvilainen 2006). We also collected imagery via flight paths that ran parallel to vineyard rows, with the sensor directed exactly nadir, thereby easing the image post-processing steps.

One VNIR flight was flown on each of the three days of field study, for a total of three high spatial resolution flights, spanning the growing season from mid-June to mid-September. Flight locations were selected based upon the presence of a significant gradient elevation, with the expectation that such terrain would provide a gradient of vine stress.

Figure 3.1. Our study used two Matrice 600 multi-copters, both equipped with Headwall hyperspectral imaging sensors. One of the on-suite sensors covered the VNIR regime from 400-1000 nm, while the other covered the SWIR regime from 1000-2500 nm. We focused on initial analysis of the VNIR flights in this manuscript.

Two locations were identified in an East-West sloping vineyard at Fox Run, where the vine rows ran North-South. Several rows of mature Cabernet franc vines were selected at a higher elevation location known to have shallower soil, and at a lower elevation location known to have heavier soil, with silt loam present in both cases. Previous work in these locations has documented clear differences in drought stress during dry periods. Standard grower management was applied in both locations.

We employed a Scholander pressure chamber, used to monitor water status of the vines, in order to calibrate our spectral data collected from the air to more traditional in-field measurements of plant stress. A Scholander pressure chamber measures the tension that has developed in leaves

when placed under a water stressed condition (N. C. Turner 1988). Specifically, we enclosed and sealed selected healthy, mature leaves inside aluminum foil-covered plastic bags, while leaves remained on the plant, as shown in Figure 3.2 below (Begg and Turner. 1970). This treatment remained in place for a minimum of 45 minutes to stop water loss from the leaf, and thus, allowing for the equilibration of the leaf with the internal plant-level water status. The leaf was then removed, placed in a thin plastic bag, sealed into a pressure chamber with the leaf stem extending through a gland, and the pressure raised slowly until water was seen at the cut end of the leaf stem. The resultant measured parameter is known as stem water potential (ψ_{stem}), and is expressed as a negative pressure value, often in the units of megapascal (MPa) or bars. Stem water potential has been found to be the best general measurement of water status in grapevines at any time (C. van Leeuwen, Pieri, and Vivin 2010).

(a) (b)

Figure 3.2. Our study used the field parameter stem water potential (ψ_{stem}) to directly measure vine water content at time of flight. (a) Leaves were bagged for at least 30 minutes prior to flight to allow for equilibration of leaves with vine plant; (b) A pressure chamber was used to capture real-time ψ_{stem} for 56 individual vine plots

Two locations were identified in an East-West sloping vineyard at Fox Run, where the vine rows ran North-South. Several rows of mature Cabernet franc vines were selected at a higher elevation location known to have shallower soil, and at a lower elevation location known to have heavier soil, with silt loam present in both cases. Previous work in these locations has documented clear differences in drought stress during dry periods. Standard grower management was applied in both locations.

Individual leaves in selected flyover locations were bagged in advance of each flyover. Circular reference markers were placed between rows, adjacent to sampled vines, to facilitate identification of sampled locations during post-processing. Since the water status of vines is known

to change and respond to weather conditions, we timed the flyover and measurement of ψ_{stem} to occur in as stable, sunny conditions as possible, as variable radiation can affect vine water status. As soon as a given UAS flyover was completed, the vine water status measurements were performed within 10 minutes at each location.

Due to the high level of rainfall in the test area over the 2018 season, no significant water stress was measured with the greatest measured stress of about -7.0 bars, or 0.7 MPa. This is a limitation in the model development as a greater stress is needed to induce significant effects on vine growth or product quality.

3.4.3 Data processing

Processing of the sUAS imagery was largely completed in ENVI®(V5.5), the image analysis software provided by the Harris Corporation. The individual frames for a given vineyard block were mosaicked using the georeferenced mosaicking function in ENVI®. Upon orthorectification of individual frame shots captured during sUAS flights, frames are provided with underlying spectra in terms of raw digital count. The six mosaics associated with VNIR flights in this study were normalized to reflectance using the atmospheric correction packages available in ENVI®, to express all data in a normalized space that accounts for atmospheric variation and enables comparison of all VNIR flights, irrespective of varying illumination conditions. We utilized the 2-Point Empirical Line Method (ELM) to convert imagery to the reflectance space. ELM is largely considered one of the most proven and reliable means of converting spectral imagery to the reflectance space (Roberts 1985). The calibration method facilitates conversion to reflectance by establishing a linear relationship between, in this case, digital count and known reflectance. Known reflectance curves were provided by means of in-scene calibration panels; it is recommended that these panels cover varying brightness levels, be homogenous, and be placed flat upon the ground (Smith and Milton 1999). We used at least two panels, one light and one dark, as shown in Figure 3.3, and measured the reflectance curves of panels, either just before or just after each flight, using a Spectra Vista Corporation (SVC) HR-1024i spectroradiometer (SVC 2019). When possible, we used more than two calibrations panels, dispersed throughout the extent of the vineyard.

Figure 3.3. We used the established 2-Point ELM to convert our imagery to reflectance. Around time of flight, we captured known reflectance curves of in-scene calibration panels, light and dark, via an SVC spectroradiometer.

We used the Spectral Angle Mapping (SAM) classifier technique in order to identify and extract vine pixels from our mosaics for complex vineyard scenes. Our aim was to extract only vine pixels, i.e., no background, soil, or heavy shadow pixels, for use in subsequent modeling efforts, since these pure vine pixels are likely to contain the useful physiological information that will facilitate linking field- and UAS-based observations. The vertically trained nature of the vines results in very narrow cross section when viewed from the nadir angle, as shown in Figure 3.4. The SAM classifier works by comparing the angle between the desired endmember (target) spectrum vector and all other pixel vectors in n-dimensional space, to select those pixels most spectrally similar to the desired endmember, i.e., vine pixels for our purposes (Kuching 2007). The threshold associated with the allowed angular difference between pixels can be adjusted to be more or less strict, as shown in Figure 3.5; we used a strict threshold of 0.001 to be certain that we captured only pure, sunlit vine pixels for analysis. The average of all extracted pixels for a given field plot was taken to be a representative spectrum for that field plot; thus, 56 spectral curves or vectors, associated with 56 vine plots, were measured during VNIR flights.

Figure 3.4. The complex nature of the vineyard necessitated the extraction of pure (sunlit) vine pixels for modeling. The tall, narrow, vertically trained vines made for small cross section in view of the sUAS platform directly above. Orange markers were placed at those locations that had field measurement taken at time of flight to facilitate post-processing.

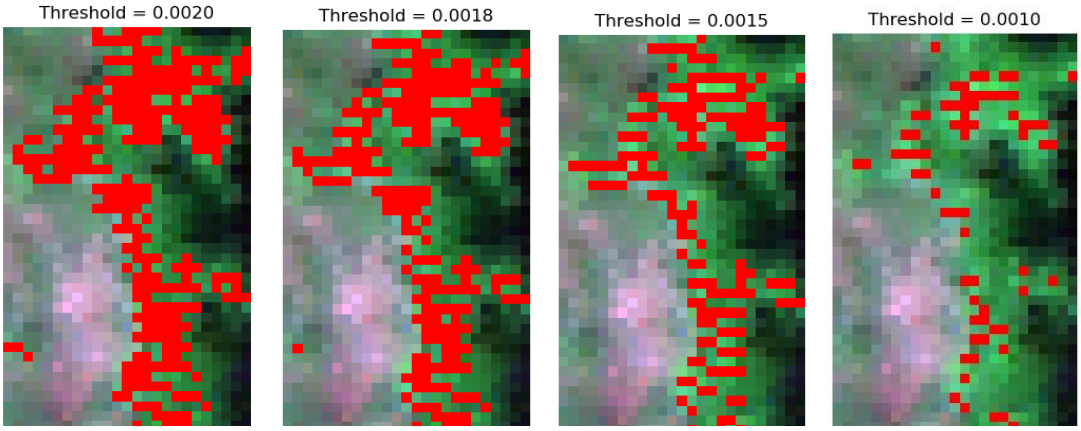

Figure 3.5. The Spectral Angle Mapping (SAM) classifier allows for accurate extraction of vine pixels from our imagery. By adjusting the allowed angular difference associated with the classifier, as shown in (a) through (d), one can be more or less strict with what is extracted in the classification. We chose a strict threshold, as shown in example in (d), for our purposes. We generated representative spectra by averaging all the extracted pixels in a plot.

Microsoft Excel was used for data formatting, after which data were analyzed in Python as a pandas data frame. Many hyperspectral analysis approaches require spectral smoothing in order to reduce extraneous noise while, at the same time, preserving critical local absorption features (Schmidt and Skidmore 2004). The Savitzky-Golay smoothing filter has become commonplace for robust smoothing of hyperspectral data during analysis efforts (Savitzky and Golay 1964). This smoothing filter fits a selected degree polynomial, usually of low degree, to successive and adjacent points across a curve using the linear least squares procedure. The Savitzky-Golay filter is often preferred for local smoothing of fine spectral curves, due to its ability to target and remove noise while maintaining local spectral features that are true to the signal. We performed tests with and without smoothing via the Savitzky-Golay filter, in order to evaluate whether local smoothing of our spectral vectors would improve modeling efforts. In parameterizing our filters, we followed the advice of recent hyperspectral spectroscopic work, and used second order polynomials with a filter size of 15 for local fitting (Prasad et al. 2015). Figure 3.6 below shows representative spectral curves, in terms of reflectance, both before and after smoothing.

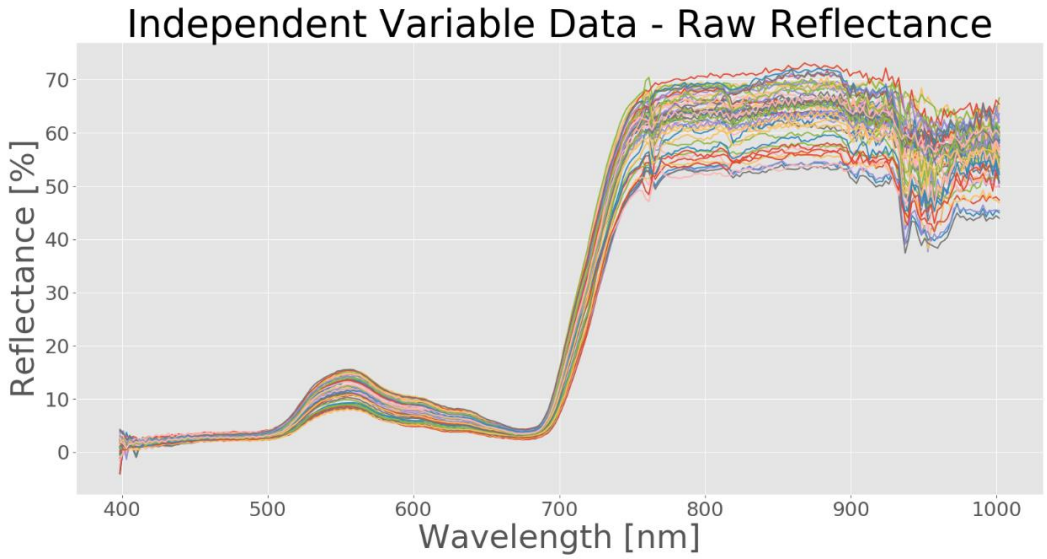

(a)

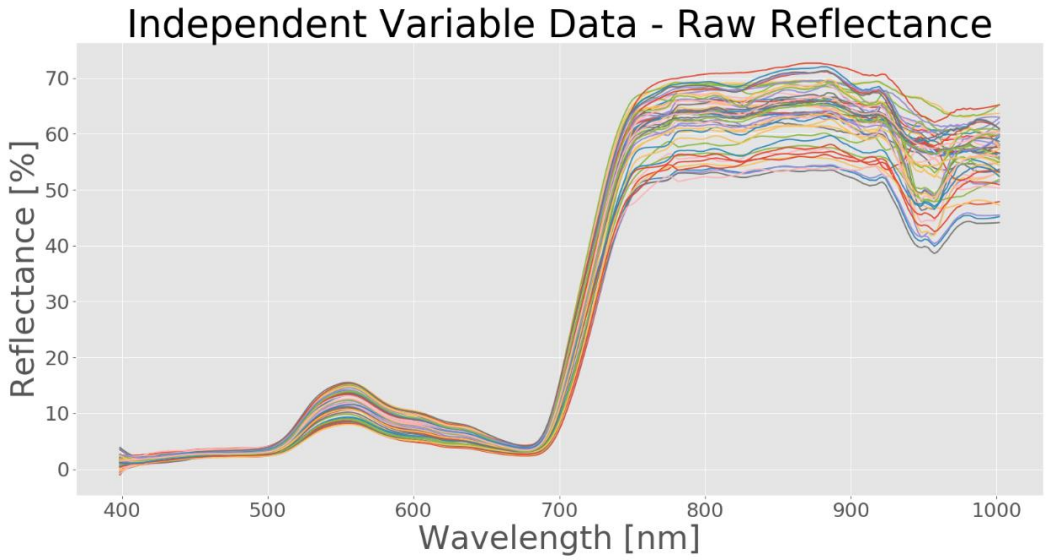

(b)

Figure 3.6. We applied a Savitzky-Golay smoothing filter to our spectral curves to explore how local smoothing could affect the efficacy of our modeling. Provided in this figure are the 56 spectral curves of vine pixels measured for water stress, normalized to reflectance, (a) before and (b) after application of the Savitzky-Golay filter.

We subsequently computed the signal-to-noise ratio (SNR) for our spectral data to evaluate the signal vs. noise levels in our UAS imagery. SNR was simply computed by taking the ratio of the mean to standard deviation, based on wavelength band. This computation is visualized in Figure 3.7 below. As the SNR is relatively low in the region of 400-450 nm, we

evaluated our models with the full range of the spectra, from 400-1000 nm, as well as for the spectral range excluding the low SNR region.

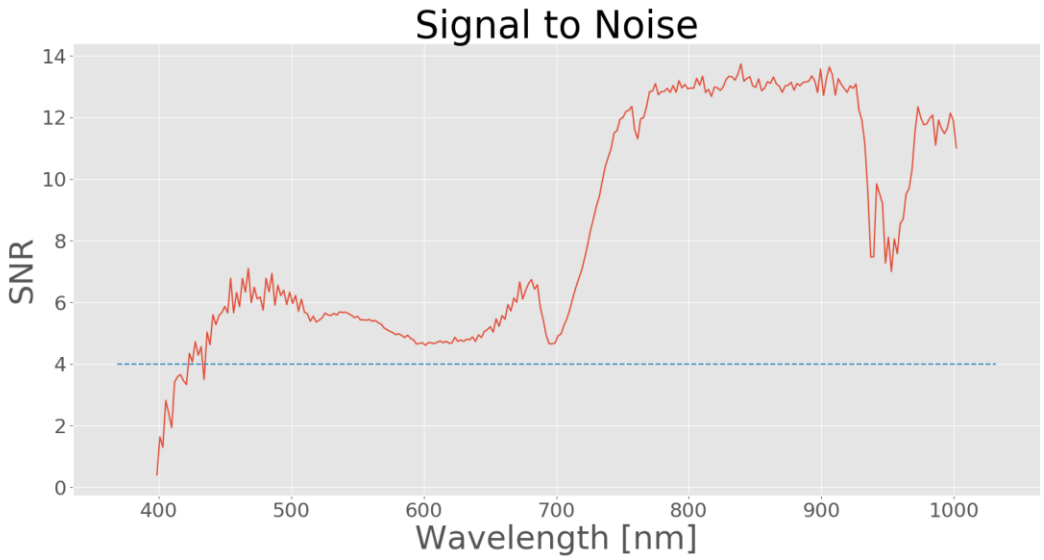

Figure 3.7. We computed the SNR of our spectral curves in order to assess true signal vs. underlying noise. Note that the SNR is relatively low for the region from 400-450 nm; we display a threshold at SNR equal to 4 in the figure. As such, we evaluated our models with the full range of spectra, while also excluding the low SNR region in a subsequent analysis.

There do not seem to be immediately obvious trends present if we color code our spectral curve plot in an attempt to separate the curves into various classes, based upon their associated SWP ground measurement (Figure 3.8). This was attributed to the lack of significant variation in the SWP measurements, i.e., the narrow SWP range, underlying the spectral data. We arguably would have observed greater separation in the spectral curve plot - some evident visual trends may have emerged when looking at moisture classes - if greater variability in the SWP model ground parameter were present. In our case, we must rely on modeling results to demonstrate statistically significant trends.

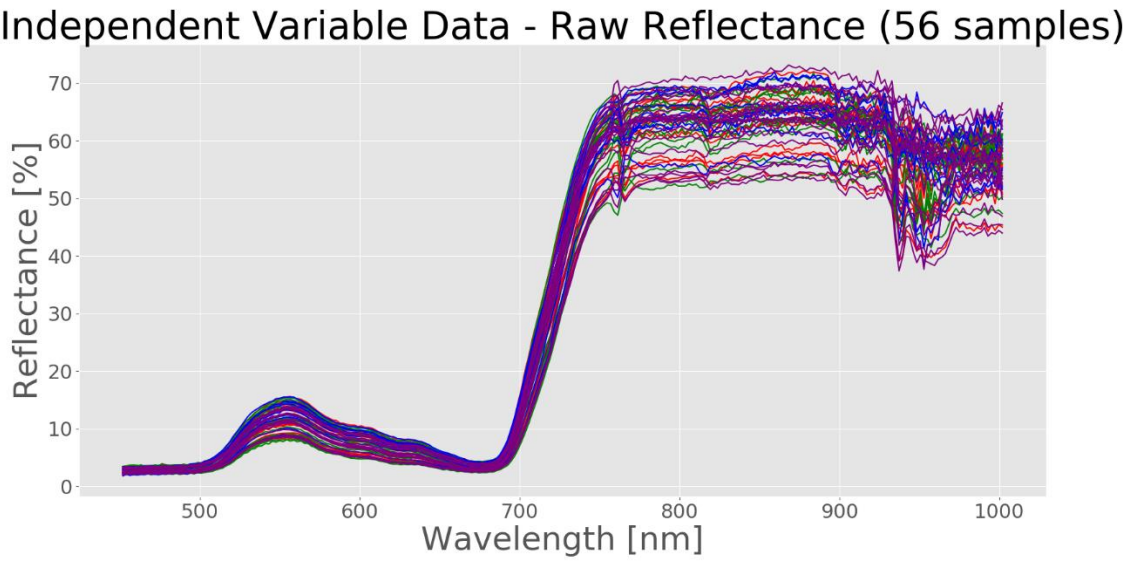

Figure 3.8. We can color code our spectral curve plots across the VNIR wavelengths, to try to separate the curves into various classes based upon their associated moisture ground measurement. We color code the 56 spectral curves into four classes: red for -3.9 to -4.4 bars, green for -4.5 to -4.7 bars, blue for -4.8 to -5.1 bars, and purple for -5.1 to -6.9 bars. There are no immediately obvious trends in the spectra, based on their classes, since there was no significant variation in the measured stem water potential.

3.4.4 Modeling methods

Although hyperspectral data of vegetation often provide insight into unique physiological indicators, given the data type's fine spectral granularity, it is often quite difficult to isolate the right bands that allow for robust, well-fitted models. Hyperspectral curves contain hundreds of, often highly correlated and redundant, predictor variables; most often, the number of predictor variables is significantly greater than the number of physiological or response variables. This generates the need for a modeling approach that can reduce data dimensionality, remove the noise associated with highly correlated variables, and identify wavelengths of greatest importance to explain the behavior in the dependent variable (Thenkabail, Lyon, and Huete 2011). We selected partial least squares-regression (PLS-R) as our modeling method of choice to overcome these challenges (De Bei et al. 2011; Santos and Kaye 2009).

PLS-R is a matrix transformation technique that minimizes the covariance between predictor variables while, at the same time, maximizing the covariance between predictor variables and response. It is distinct from principal component regression, since it accounts for both predictor and response variables, by way of both inner and outer matrix transformations (Geladi and Kowalski 1986).

The predictor variable data block can be linearly transformed as

$$\boldsymbol{X} = \boldsymbol{TP}' + \boldsymbol{E} = \sum \boldsymbol{t_h p'_h} + \boldsymbol{E}$$

where **X** is the matrix of predictor variables, **T** is a projection of **X** as components, **P** is a loading matrix containing factor scores, and **E** is a matrix of error terms.

The response data block, our ψ_{stem} measurements, can be similarly deconstructed into

$$\boldsymbol{Y} = \boldsymbol{UQ}' + \boldsymbol{F} = \sum \boldsymbol{u_h q'_h} + \boldsymbol{F}$$

where the transformations are the same as those for the predictor variables.

PLS-R analyses for this study were completed in Python using the PLSRegression package in the Scikit-learn machine learning library ("Scikit-Learn" 2019). Data run through the PLSRegression package are automatically mean-centered, that is, centered to the mean and scaled to unit variance on a component-wise basis (Geladi and Kowalski 1986). The quantity of latent variables (LV) was determined by optimizing for the mean square error (MSE) of prediction; i.e., the number of LVs which minimized MSE was selected for a given model (Rapaport et al. 2015).

While the use of PLS-R serves to remove the noise associated with high covariance, we also required a method for identifying wavelengths of importance in a variable selection scheme. Previous studies have used variable importance in projection (VIP) and used a VIP-statistic score (threshold) for removing less important wavelengths and thus optimize model performance (Rapaport et al. 2015). This work more plainly recognized the vector of regression coefficients, used to perform the PLS-R, as an indicator of the association between predictor variables and response (Mehmood et al. 2012). Variables, or wavelength bands, with lower absolute regression coefficients have lower relative correlation, or ability to explain, the response ψ_{stem}. We therefore iteratively removed wavelengths with the lowest absolute regression coefficients from consideration, until the MSE of prediction no longer improved upon recalibration of a given model (Andersen and Bro 2010).

3.4.5 Statistical analysis

We considered model performance in context of our smoothing procedure, as well as our SNR thresholding. Thus, we noted model performance for: the full spectral range of 400-1000 nm, with and without smoothing, and the reduced spectral range of 450-1000 nm, with and without

smoothing. We reviewed the number of LVs, coefficient of determination (R^2) for calibration, coefficient of determination (R^2) for cross-validation, root mean squared error of calibration (RMSEC), and root mean squared error of cross-validation (RMSECV) to assess model performance (Rapaport et al. 2015). For cross-validation, we used a k-folds cross-validation procedure with five folds. We expected a strong model to have a low number of LVs, high R^2 metrics, and low MSE metrics.

3.5 RESULTS

3.5.1 Latent variables

The quantity of LVs, or PLS-R components used to build a regression for a given model, was determined by selecting the number of LVs which minimized MSE. Using the raw reflectance data frame, with associated ψ_{stem} field measurements, we ran our PLS-R regression with a variable number of LVs, up to a maximum of 25. We recorded the RMSECV associated with each model run, and selected the number of LVs, for a given model, which yielded the lowest RMSECV.

We found that all variations of our data set, before and after variable selection efforts, considering spectral smoothing and wavelength range, were optimized with a relatively low number of LVs. For example, before variable selection, the largest quantity of LVs selected was for the smoothed data for the full spectral range from 400-1000 nm and was optimized with 10 LVs. Figure 3.9 below demonstrates the selection of LVs for smoothed and unsmoothed spectral data for the range of 400-1000 nm. When model performance first increases and then decreases with additional LVs, as can be seen with our model runs demonstrated in Figure 3.9, it is a strong indication that using too many or suboptimal number of LVs could overfit the data and not yield robust models. We therefore were careful to select the optimal number of LVs for our reported model results.

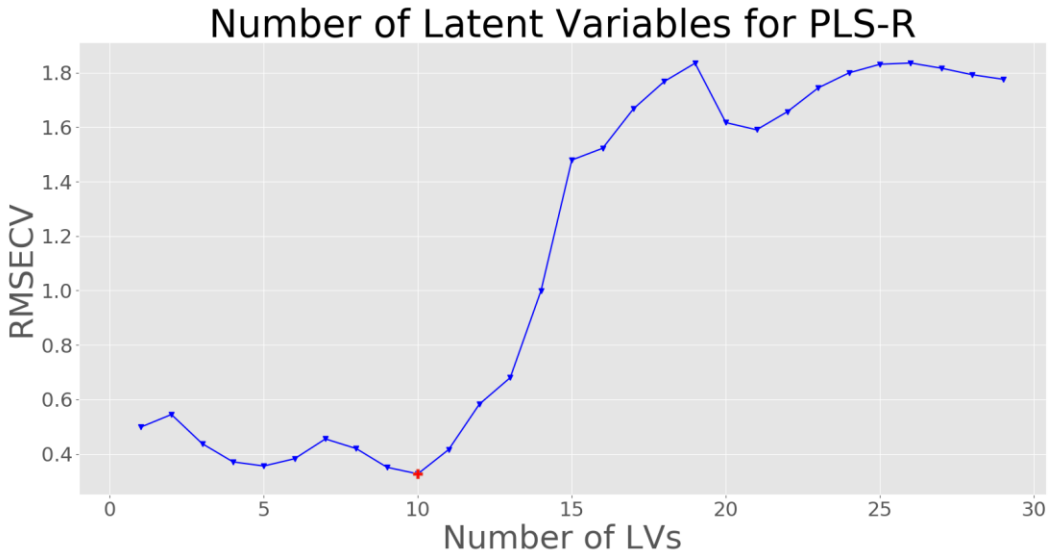

(a)

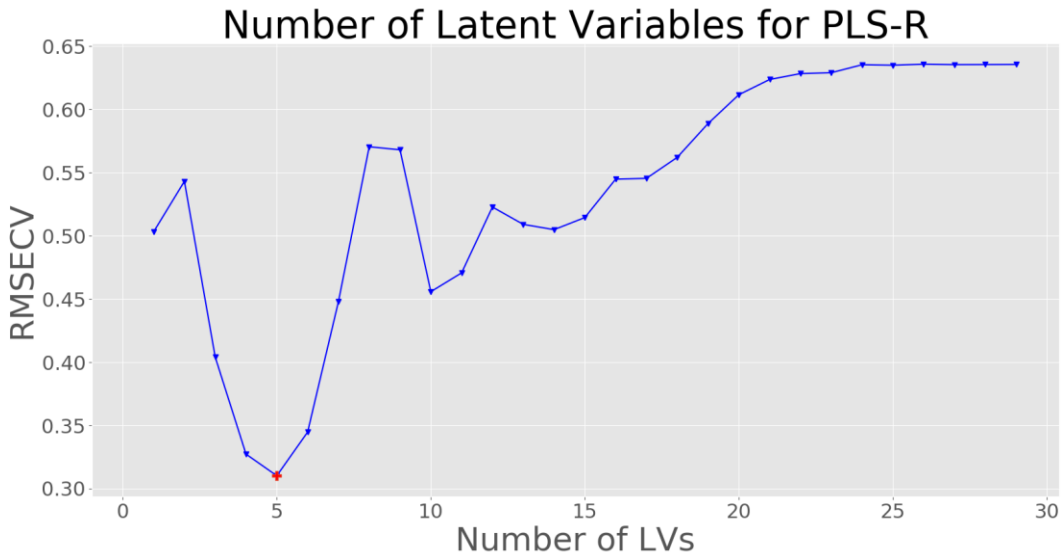

(b)

Figure 3.9. Using the raw reflectance data frame and associated ψ_{stem} field measurements, we ran our PLS-R regression with a variable number of LVs, up to a maximum of 25. We selected the number of LVs, for a given model, which yielded the lowest RMSECV. All variations of our considered data sets were optimized with a relatively low number of LVs; e.g., for the range of 400-1000 nm, (a) the smoothed data used 10 LVs and (b) the unsmoothed data used 5 LVs.

3.5.2 PLS-R analyses

As previously mentioned, we optimized the number of LVs and wavelength band variables for four separate data setups: smoothed and unsmoothed data for both the ranges of 400-1000 nm

and 450-1000 nm.

Figure 3.10 shows the regression fits for the smoothed and unsmoothed data for the range of 400-1000 nm, while Figure 3.11 shows the regression fits for the smoothed and unsmoothed data for the range of 450-1000 nm. Figure 3.12 provides an example of how we can visualize the wavelength bands that were selectively discarded from consideration in the calibration of a given model. Table 3.1 summarizes the relevant model performance metrics for the four data setups considered.

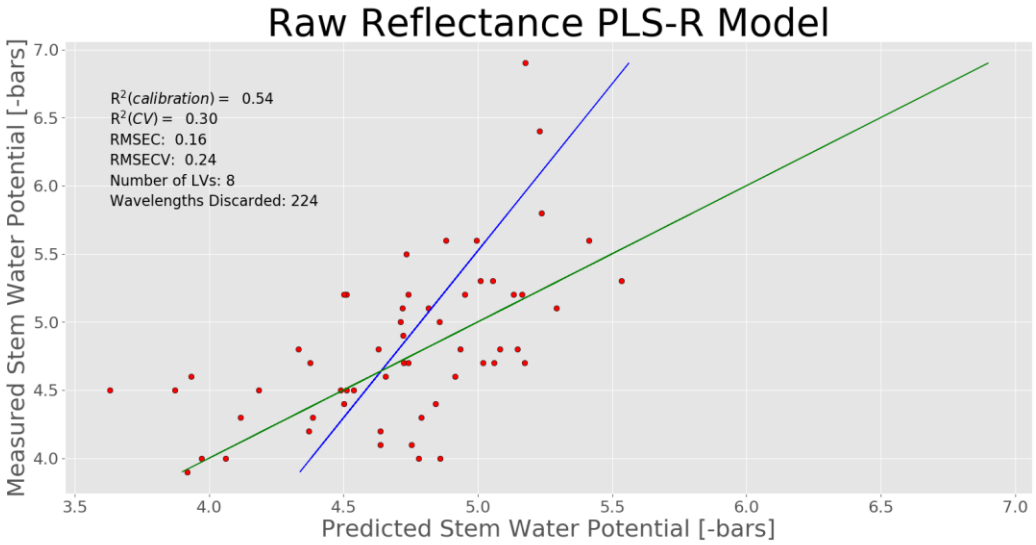

(a)

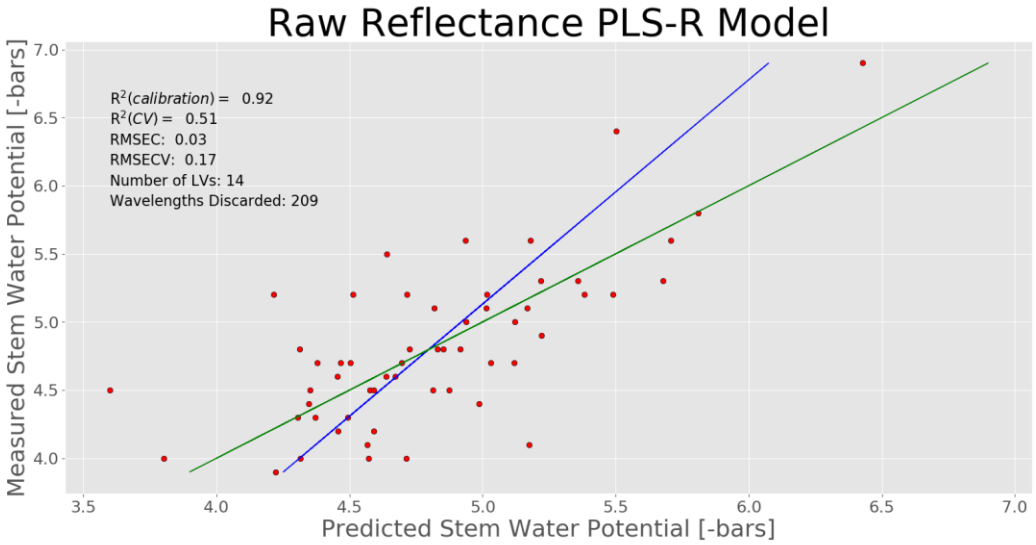

(b)

Figure 3.10. The optimization of latent variables and wavelength band selection for the smoothed and unsmoothed data for the range of 400-1000 nm. The R^2 cross-validation metric (CV) for (a) the smoothed data was 0.30 and for (b) the unsmoothed data was 0.51.

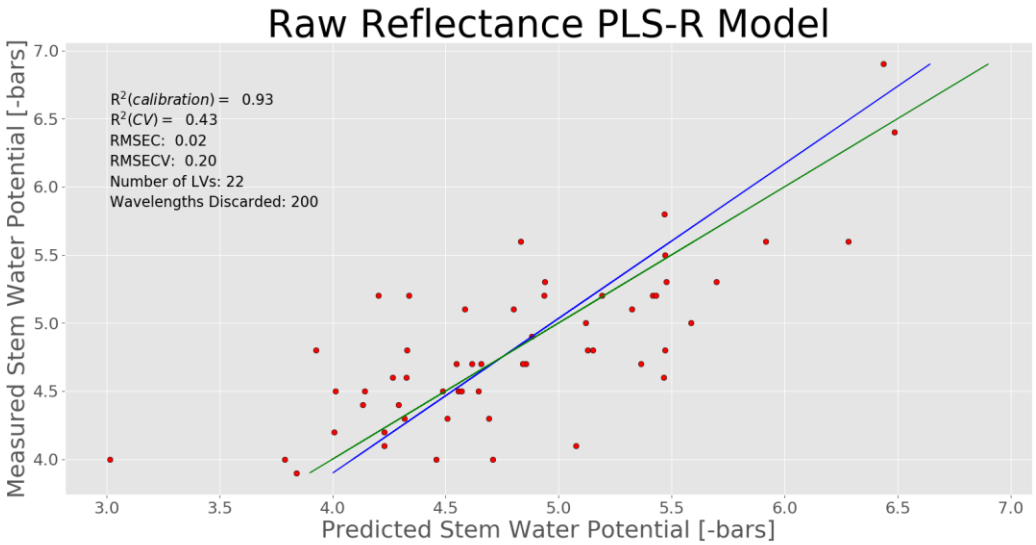

(a)

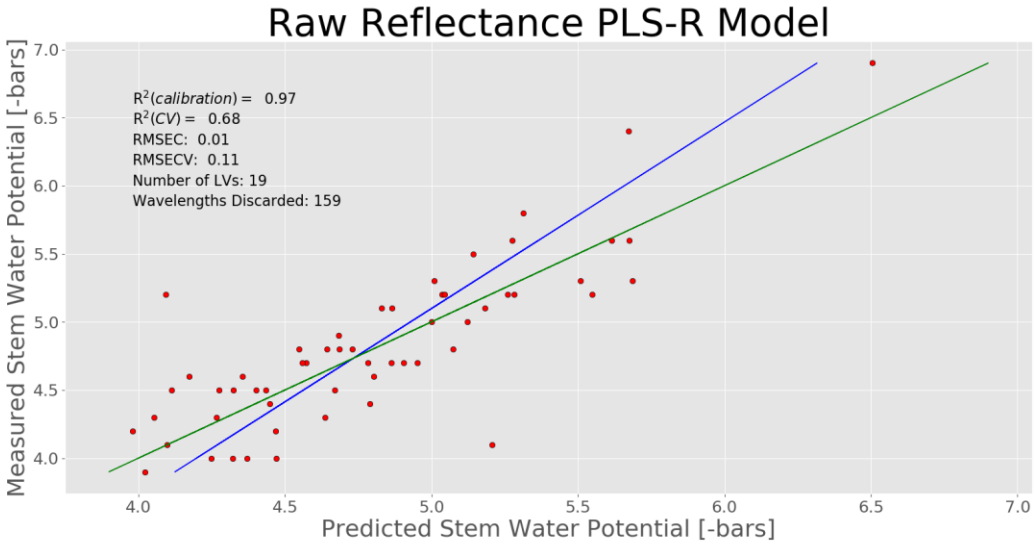

(b)

Figure 3.11. The optimization of latent variables and wavelength band selection for the smoothed and unsmoothed data for the range of 450-1000 nm. The R^2 cross-validation (CV) metric for (a) the smoothed data was 0.43 and for (b) the unsmoothed data was 0.68.

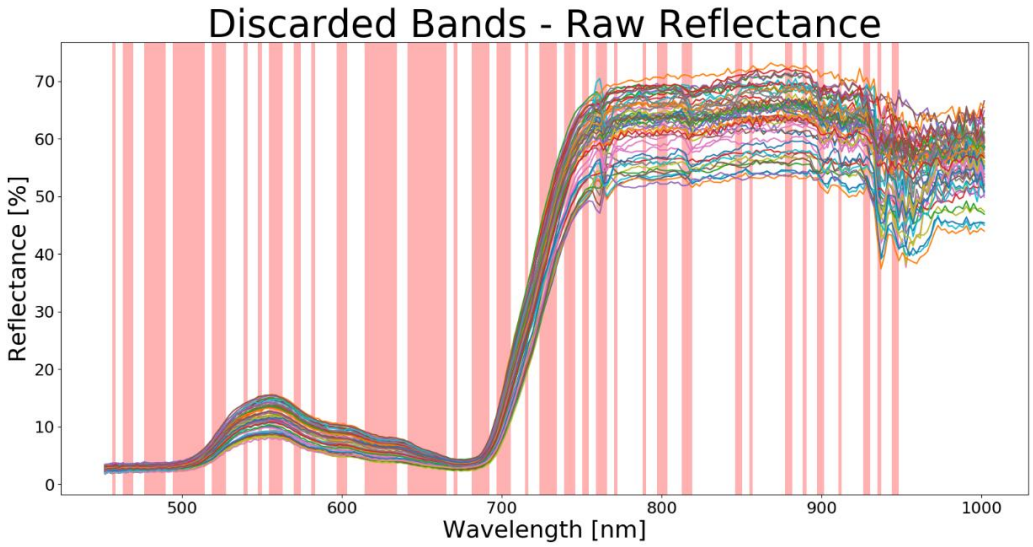

Figure 3.12. We can visualize which wavelengths have been selectively discarded from consideration in the calibration of our models. In the case of the unsmoothed data, for the range of 450-1000 nm, we discarded 159 of the original 270 wavelengths. Areas with light red background are those bands which were not considered in calibration, since they were shown to be lower in explanatory power.

Table 3.1. Summary of the PLS-R model performance metrics for the four data setups we considered. The narrower 450-1000 nm regime (removal of the low SNR bands) always performed better than the full spectral range. Furthermore, smoothing of the spectral data via the Savitzky-Golay filter reduced model performance. The difference between the calibration and cross-validation coefficients of determination is explained by the fact that the data sample size is relatively small.

Spectral Range	**Spectral Smoothing**	**R^2 for Calibration**	**R^2 for Cross-Validation**
400-1000 nm	Yes	*0.54*	*0.30*
400-1000 nm	No	*0.92*	*0.51*
450-1000 nm	Yes	*0.93*	*0.43*
450-1000 nm	No	*0.97*	*0.68*

The best performing model was the unsmoothed data for the 450-1000 nm range and the worst performing model was the smoothed data for the 400-1000 nm range, considering R^2 (CV) as the metric of choice for comparison assessment. Spectral smoothing, via the Savitzky-Golay filter, consistently reduced model performance. The full spectral range (400-1000 nm) furthermore diminished performance, when compared to cases when the low SNR range (400-450 nm) was removed.

Even though we parameterized our smoothing filters based on results from recent hyperspectral studies, using second order polynomials with a filter size of 15 for local fitting, the spectral smoothing had an adverse impact on model performance in all cases. We attributed this outcome to the fact that, while the smoothing operation served to remove some noise in the spectra, the operation also suppressed local spectral absorption features, some of which proved paramount in our modeling efforts. For example, it seemed that the smoothing operation reduced the O_2 absorption feature near 750 nm and smoothed the intricate NIR regime to an excessive extent, based on visual inspection (Figure 3.6). It would be prudent to either further study the parameterization of an appropriate smoothing filter or to avoid smoothing altogether; this is an area that arguably warrants more study.

We tested our models with both the full spectral range and absent the low SNR region (400-450 nm) in order to better understand the impact of higher noise presence in the shorter wavelengths. It was clear after running our models that the underlying noise in the shorter wavelengths had a seemingly large impact on model performance. Considering that the noise at the extreme ends of the spectral range could likely be traced to the atmospheric calibration of the spectra, a more advanced technique than ELM may be worth exploring. This result also hints at the importance of computing SNR for a given data set to better understand the data set's noise characteristics.

In further reviewing the summary model performance results (Table 3.1), it is evident that the R^2 (CV) metric was always lower than the more traditional R^2 (calibration) metric. This effect was not surprising considering that the k-folds CV procedure is much more rigorous than computation of the traditional metric, since it tests a given model on an independent, internal partition of the data set. The R^2 (CV) metric thus provides a more robust indication of how a given model would perform if completely new, independent data were considered. The relative difference between the calibration and cross-validation coefficients of determination is explained by the fact that the data sample size is relatively small, with only 56 samples to model; an expansion of the sample data set potentially could reduce the relative difference between our two R^2 metrics.

3.6 FUTURE WORK

This study represents our initial investigation and results into the use of sUAS-based hyperspectral imagery for assessment of vineyard moisture status. We contend that future efforts could focus on expanding the wavelength range, optimizing the selection of predictor variables, and providing more detail on the link between selected wavelengths and plant physiology.

3.6.1 SWIR data

We completed flights with both VNIR and SWIR sensors during the airborne campaign; flights with the SWIR sensor directly followed the VNIR flights. The results presented in this manuscript only considered data collected during the VNIR flights. Future work will follow similar methodology presented in this manuscript to expand the spectral range to 400-2500 nm, thereby enabling a more exhaustive analysis. Many other studies on grapevine water status assessment have pointed to the SWIR regime as important in the prediction of water status (Maimaitiyiming et al. 2017; De Bei et al. 2011; Rapaport et al. 2015).

3.6.2 Wavelength band selection

In this study we optimized our models with a variable selection scheme that removed less explanatory wavelength bands, given associated regression coefficients. Models often were optimized by removing more than 200 of the original 270 spectral bands collected. It may be worthwhile in future efforts to limit the number of wavelengths to the number and range which could be accommodated by a cheaper, simpler multispectral sensor. For example, the Tetracam Macaw camera series includes options for six or 12 user-selected spectral channels.

3.6.3 Physiological links

It is well understood that a predictive model in an environmental remote sensing application could only truly be characterized as “robust” if it utilizes variables that have physiological meaning, over and above strong predictive power. We therefore will confirm that the predictor wavelengths have some associated physiological meaning, in collaboration with plant physiologists. It could be argued that an end user of research-based models, such as a local vineyard manager, will only trust predictive tools that can be explained by factors well understood at the operational level. This must also provide proven enhancements in grape and vine quality to justify changes in management such as differential harvest or developing precision irrigation.

3.7 CONCLUSIONS

This study examined the effectiveness of using hyperspectral data, collected via sUAS platform, for the purposes of accurately estimating real-time water status in grapevine. Whereas many previous studies have examined the use of sUAS or in situ hyperspectral sensing for observing grapevine water status, the current work bridged the gap between the two sensing levels. High-spatial resolution hyperspectral data were collected over an Upstate New York vineyard over three flight days, along with traditional field measurement of midday stem water potential (ψ_{stem}) at time of flight. A partial least squares-regression (PLS-R) modeling method was used to correlate flight collected spectra and field measurements. With the consideration of model parameter optimization and a variable selection scheme, we showed model performance as high as R^2 (CV) = 0.68. Model performance was dependent on the smoothing and SNR data reduction applied, where unsmoothed spectral data and a reduced spectral range, respectively, performed better. Considering the limited range of stress we encountered, the modeling performance achieved is promising for the use of sUAS and hyperspectra in vineyard evaluation, and supplementary research efforts. Future work will seek to include flight data collected in the SWIR spectral regime, improved explanation of physiological links, and additional steps towards operationalizing commercial technology applications. While these models will require independent validation over a much larger range of vine stress, results such as these bode well for the application of sUAS-based spectral sensing of vineyard moisture status, given the high value of the crop and relatively fine scale of the management needs.

Chapter 4

Combining hyperspectral imaging and small unmanned aerial systems for grapevine moisture stress assessment

4.1 FOREWORD

This chapter further expands upon the results of Chapter 3 by including the SWIR data collected in the field and discerning links to plant physiological phenomena. This chapter will be submitted to *Precision Agriculture* (PRAG) and addresses Objectives 2, 3, 4, and 5.

4.2 ABSTRACT

It has been shown that mild water deficit in grapevine contributes to wine quality, in terms of especially flavor. Water deficit irrigation and selective harvesting are implemented to optimize quality, but these approaches require rigorous measurement of vine water status. While traditional in-field physiological measurements have made operational implementation onerous, modern small unmanned aerial systems (sUAS) have presented the unique opportunity for rigorous management across vast areas. This study sought to fuse hyperspectral remote sensing, sUAS, and

sound multivariate analysis techniques for the purposes of assessing grapevine water status. High-spatial and -spectral resolution hyperspectral data were collected in the visible/near-infrared (VNIR; 400-1000nm) and short-wave infrared (SWIR; 950-2500 nm) spectral regions across three flight days at a commercial vineyard in upstate New York. A pressure chamber was used to collect traditional field measurements of stem water potential (ψ_{stem}) during image acquisition. We correlated our hyperspectral data with a limited stress range (wet growing season) of traditional measurements for ψ_{stem} using multiple linear regression (R^2 between 0.34 and 0.55) and partial least squares regression (R^2 between 0.36 and 0.39). We demonstrated statistically significant trends in our experiment, further qualifying the potential of hyperspectral data, collected via sUAS, for the purposes of grapevine water management. There was indication that the chlorophyll and carotenoid absorption regions in the VNIR, as well as several SWIR water band regions warrant further exploration. This work was limited since we did not have access to experimentally-controlled plots, and future work should ensure a full range of water stress.

4.3 INTRODUCTION

It has been shown that environmental conditions have a significant impact on grape quality (flavor, acidity, sugar content, etc.), which has led to crop management interventions being leveraged to positively impact quality (Cornelis Van Leeuwen and Seguin 2006). Furthermore, grapevines and associated harvest quality actually benefit from suboptimal ecological settings, particularly in reference to vine moisture status, even though this runs contrary to common convention with most agricultural crops. The presence of a mild moisture deficit in grapevines prompts a reduction in shoot growth, berry weight, and yield, all of which are factors that collectively serve to inflate berry anthocyanin and tannin levels and, as such, perceived quality (Cornelis Van Leeuwen et al. 2009). Controlled deficit irrigation thus has emerged as a means to induce mild moisture deficit stress in grapevines, and has been demonstrated to yield improved berry quality, while maintaining operationally acceptable yield (Chaves et al. 2007). Similarly, taking into consideration vineyards where deficit irrigation techniques cannot be realized, the knowledge of vine water status may dictate selective harvesting practices, giving way to ideal quality and yield (Bramley et al. 2005). However, any reasonable operational implementation of vine moisture management demands accurate, precise, and ideally, spatially-exhaustive, measurement of vine moisture status.

Management of vine moisture status traditionally has been facilitated by direct in-field measurement of sensitive physiological indicators. Stem water potential (ψ_{stem}), a measure of integral plant transpiration and an indicator of the capability for grapevines to conduct water from the soil to the atmosphere, has been validated as one such sensitive indicator that may aid vine moisture management (Chone et al. 2001). The practice of gauging ψ_{stem} at midday is particularly alluring, as it grants insight to moisture status at time of peak plant transpiration activity. A pressure chamber typically is used to measure the negative pressure in the xylem of plants in order to gauge the underlying ψ_{stem} associated with a given vine (Scholander et al. 1965). While strides have been made in numerous vineyard settings to operationally respond to in-field measures of vine moisture status, accurate measurements often require an inordinate amount of time and labor, and progress in operational application remains gradual (Rodríguez-Pérez et al. 2007).

It is in this context that remote sensing technology has become an increasingly common tool to remotely probe for plant physiological indicators, like plant moisture status, via observations of the unique (electromagnetic) spectral response related to plant moisture regimes. The potential superiority of non-destructive remote sensing techniques, for these purposes, lies in the cost-effective, highly productive, and objective nature of application (Govender et al. 2009). Significant progress in the spectral and spatial granularity of enabling sensors has made the operational implementation of such sensors for precision field application more tenable. In the visible (VIS) regime of the spectrum, i.e., 400-700 nanometers (nm), and the near infrared (NIR) regime, 700-1000 nm, subtle variations in photosynthetic pigments, such as chlorophyll and carotenoids, and leaf structure variations are evident (Josep Peñuelas and Filella 1998). In the short-wave infrared (SWIR) regime, i.e., 1000-2500 nm, several strong atmospheric absorption bands are present and vegetation moisture content dominates as the primary influence of plant spectral signatures (Behmann, Steinrücken, and Plümer 2014). This marriage of remote sensing and grapevine moisture status monitoring therefore has been examined and has shown promise (Möller et al. 2006; Rodríguez-Pérez et al. 2007; Acevedo-Opazo et al. 2008; Serrano, González-Flor, and Gorchs 2012; Baluja et al. 2012; Bellvert et al. 2014; Pôças et al. 2015; Maimaitiyiming et al. 2017; Loggenberg et al. 2018; Zovko et al. 2019).

Many past studies have applied a library of existing spectral narrow-band indices (e.g., the normalized ratio of two wavelengths), thereby isolating a few spectral bands to relate to underlying

plant physiological phenomena. However, the universal nature of established spectral indices typically ignores the unique disposition of spectral responses amongst distinct plant species of interest and their environment terroir (Rapaport et al. 2015). Furthermore, Zovko et al. (2019) stated that the reliance on spectral indices may pose the risk of neglecting otherwise useful information, inherent in the fine spectral character of modern hyperspectral sensors. The strict study of a specific species, like various grapevine varieties, for a targeted response should encourage the application of a high spectral resolution (hyperspectral) sensor and a rational downsizing to the most pertinent spectral bands, given the physiological response under investigation. Stated differently, the oversampling in the spectral domain via hyperspectral sensors (narrow, contiguous spectral channels) enables researchers to determine the subset of spectral channels required to assess specific plant physiological states, which leads to a potentially more operational multi-spectral (fewer wavelengths) solution (Delalieux et al. 2009). This informed down-selection of wavelengths via sound multivariate analysis techniques enables practitioners to leverage the high spectral resolution of modern hyperspectral sensors, while distilling the data to emphasize spectral characteristics that are most pertinent to specific applications.

Hyperspectral data, collected via in-situ spectroradiometers, have been extensively utilized in earlier vineyard moisture assessment studies, with some including only the VIS and NIR and others the more comprehensive VNIR-SWIR range. For example, Rodríguez-Pérez et al. (2007) related hyperspectral reflectance data (350-2500 nm) collected in a commercial vineyard of Pinot noir, using an integrating sphere and field spectrometer, to numerous reflectance indices and used the data to perform continuum removal analysis (Kokaly and Clark 1999). The authors evaluated the difference between midday ψ_{stem} and pre-dawn leaf water potential, and achieved strong fits with the Red/Green Index ($R^2 = 0.619$) and the structure intensive pigment index ($R^2 = 0.541$). They reported a fit of $R^2 = 0.509$ for the continuum removal analysis, using the maximum band depth at the minor water absorption feature at 970 nm. Serrano et al. (2012) used a spectroradiometer covering 400-1100 nm to capture spectral data of leaves in a rainfed vineyard across 256 spectral channels. They aimed to investigate the relation between the normalized difference vegetation index (NDVI) and berry yield/composition during mild to moderate moisture stress. They found NDVI to reasonably model total soluble solids ($R^2 = 0.81$) and maturity index at harvest ($R^2 = 0.89$), while the Water Index performed well with regards to titratable acidity ($R^2 = 0.62$) and maturity index ($R^2 = 0.67$). Similar to Rodríguez-Pérez et al. (2007), Rapaport et al.

(2015) also used an integrating sphere and field spectrometer to capture hyperspectral signatures (400-1700 nm) of grapevine leaves and used the partial least squares regression technique to identify reflectance trends related to stress. They identified opposing trends at 530-550 nm and 1500 nm, which they associated with plant pigments and leaf water content. More recently, Zovko et al. (2019) implemented four water treatments of grapevine in an experimental vineyard setting to evaluate how well they could classify treatments and to identify pertinent spectral regions, given data collected via ground spectroradiometers. In the VIS and NIR regimes, they point to changes in the chlorophyll-a to chlorophyll-b ratio as indicative of water deficient vines. In the SWIR regime, the study lists a number of wavelengths as important to the classification, particularly wavelengths in the O-H stretch in water, as well as longer wavelengths in the SWIR, related to leaf water content. The next iteration of research inevitably involved scaling results to airborne platforms.

The application of aircraft or satellite platforms as the media via which to collect plant spectral data at a precise level remains inhibitive, mainly due to shortcomings in spatial and temporal resolutions, as well as strict adherence to weather conditions. However, the ever-increasing technological base for small unmanned aerial systems (sUAS) has presented the unique opportunity for rigorous management at the plant or zone level across vast field areas. In fact, the advent of the sUAS platform for precision agriculture application arguably balances the demands for low cost, high spatial/spectral/temporal resolutions, and ease of use, and lends itself well to moisture management applications (Gago et al. 2015). Recent scholarly work in precision viticulture has supported the notion that sUAS, as the remote sensing platform of choice, warrants further exploration in the realm of grapevine water status monitoring (Baluja et al. 2012; Bellvert et al. 2014).

More recent studies in grapevine moisture stress have investigated sUAS platforms to collect plant spectral data for modeling purposes. Primicerio et al. (2012) built a sUAS platform for site-specific vineyard management at an experimental vineyard in central Italy, collecting 63 multispectral images in total. Their results included vigour maps that clearly delineated crop heterogeneity matching their ground field truth. Baluja et al. (2012) collected multispectral (six bands at 530, 550, 570, 670, 700 and 800 nm) and thermal imagery via sUAS to study water status variability in a commercial rainfed vineyard. The authors reported that the normalized difference

vegetation index (NDVI) and TCARI/OSAVI (a ratio between chlorophyll absorption and a soil-adjusted index) exhibited the best correlation with ψ_{stem}, with $R^2 = 0.68$ and $R^2 = 0.84$, respectively. It is worth noting that ground measurement of ψ_{stem} extended to greater than -14.0 bars, which led to their analysis including a relatively full range of moisture stress. Zarco-Tejada et al. (2013), on the other hand, examined the Photochemical Reflectance Index (PRI) as a proxy for water stress condition in grapevine. Their data consisted of multispectral and thermal imagery captured during four airborne collection efforts. The authors presented a novel normalized PRI, taking into consideration canopy structure and chlorophyll content. Santesteban et al. (2017) also used a sUAS platform to assess water status variations within a vineyard, but implemented high-resolution (0.09 m) thermal images for a 7.5 ha vineyard; they found the crop water stress index (CWSI) to be well correlated with stem water potential and stomatal conductance. Finally, Caruso et al. (2017) deployed a sUAS platform, equipped with VIS-NIR cameras, to investigate vineyard parameters including leaf area index, leaf chlorophyll, and canopy geometric indicators. High spatial resolution sUAS-based hyperspectral studies, however, remain scarce. Thus, there still is a need to further evaluate sUAS-based, high spatial resolution, and especially hyperspectral imagery for different geographic regions, thereby validating past efforts for different regions and grape varieties.

The overarching objective of this study therefore was to fuse hyperspectral remote sensing, sUAS, and sound multivariate analysis techniques for the purposes of assessing grapevine moisture status, for the geographical region of the Finger Lakes, NY, USA. While much work has been done to explore the use of hyperspectral data for modeling grapevine moisture status, few of these works explore the full VNIR-SWIR spectral range and even fewer collect their spectral data in an airborne campaign. This work aims to bridge this gap and work closer to a more operational solution for vineyard managers. The specific objectives for this work included (1) assessing the potential of sUAS-based hyperspectral remote sensing for managing grapevine moisture status; (2) identifying the most pertinent spectral regions for discerning grapevine moisture status; and (3) interpreting results to establish links to known plant physiological phenomena. In this work, data were collected via sUAS in the VIS, NIR, and SWIR spectral regimes, and analyzed using linear regression and partial least squares (PLS) analysis. We also will present results that are specific to the various regions, i.e., from the VIS/NIR (cheaper silicon detector range), to the longer wavelength SWIR domain, even though the latter implies additional sensor costs and data noise

considerations.

This study's original intent was to capture a level of variability in moisture status that would enable highly accurate predictive models; however, the lack of access to experimental plots with a large range in moisture stress conditions (ψ_{stem}), due to a growing season with a high level of precipitation, made this problematic. The focus of the work therefore shifted to the identification of statistically significant trends to inform past and future related efforts, specifically to assess the sensitivity of our identified spectral indicators to model narrow-range ψ_{stem}. We hypothesized that our results would confirm a statistically-significant correlation between moisture status and our spectral data, even though it may not be robust as an accurate predictive tool, due to our observed narrow-range ψ_{stem}. Given the limitations of the study, we expected to inspire future research that would further build upon trends and conclusions presented in this effort.

4.4 METHODOLOGY

4.4.1 Study area

The Finger Lakes Wine Country of Upstate New York has grown in the last few decades to include more than 4,500 hectares of planted vineyards across no less than 100 wineries throughout Upstate New York, USA (Figure 4.1). The Finger Lakes region encapsulates eleven long and narrow bodies of water, forged through glacial activity in the Pleistocene Epoch (Newman 1986). Summer seasons are ordinarily characterized by moderate, humid conditions with fluctuating rainfall; the rainfall totals in the Finger Lakes during the 2018 season, examined in this work, were above normal. Specifically, between the months of June and September (2018), the rainfall total in Penn Yan, New York, amounted to 14.74 inches (~374 mm), in contrast to a past average of 14.05 inches (~357 mm), as per the NOAA regional climate center in the area. Winters are often cold, making for short growing seasons as compared to most other viticultural regions. Though faced with difficult climatic conditions, viniculture is made possible in the region due to microclimate factors, like air draining and lake effects.

A mature, commercial vineyard on the western shore of Seneca Lake – Fox Run Vineyards – was used as the field site for this study. Fox Run Vineyards has complex soil patterns, dominated primarily by gravelly silty clay throughout most of the vineyard, and transitioning to a fertile and

well-drained sandy loam closer to the lake shore. The vineyard regularly grows five different grape varieties, namely Riesling, Chardonnay, Lemberger, Cabernet Franc, and Cabernet Sauvignon; however, our focus in this study was Cabernet Franc vines. Reminiscent of many vineyards in the Finger Lakes region, Fox Run bears its vines directly along the shore of its neighboring lake body, sloping downward towards Seneca Lake, with a minimum elevation of around 140 meters and a maximum elevation of around 210 meters above sea level (Figure 4.2a). Vine rows stretch from north to south and are vertically trained to supporting trellises (Figure 4.2b). The vineyard does not have active irrigation systems, but rather relies on careful timing of harvest. Fox Run extends an intricate terroir ideally suited for environmental studies of grapevine water.

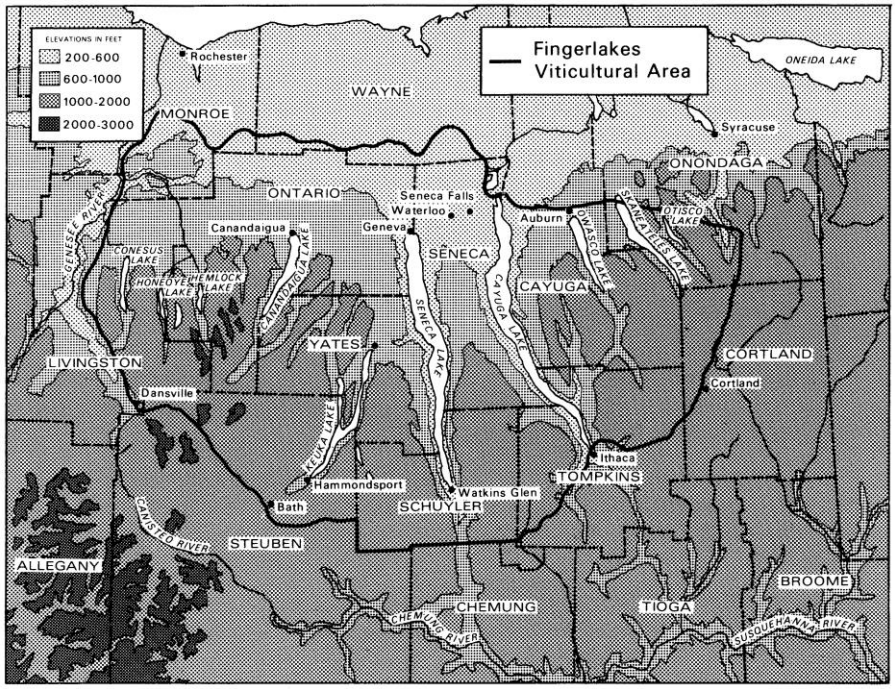

Figure 4.1. The Finger Lakes American Viticultural Area (AVA) boasts 11 glacial lakes and is prone to extreme winters and moderate, humid summers. The region sports microclimate factors, e.g., air draining and lake effects that make viticulture possible in a region otherwise not suited for such activities (Newman 1986).

(a) (b)

Figure 4.2. Our study levied a mature, commercial vineyard on the western edge of Seneca Lake in the Finger Lakes wine region of Upstate New York. (a) The vineyard exhibits a strong gradient of elevation relative to the lake edge, with elevation above sea level ranging from around 140-210 m. (b) The vines run North-South and are vertically trained to trellises.

4.4.2 Data collection

We conducted air and ground campaigns to facilitate the synthesis of hyperspectral imagery with more traditional evaluation techniques carried out on the ground; this was done in order to reliably correlate flight-collected spectral data with proven sensitive physiological indicators. All supporting data for the current study were collected across three days within the 2018 growing season, spread out from mid-June to mid-September. During these three days of data collection, sky conditions were verified as either free of cloud cover or uniformly distributed with cloud cover, thereby aiding subsequent spectral calibration efforts.

The DJI Matrice 600 multi-copter sUAS platform was as the base airframe for our flight campaigns (Figure 4.3) due to its modular efficiency (https://www.dji.com/). Trimble Applanix-15 boards were implemented in the designs to further boast the direct georeferencing and inertial intelligence of the sUAS platforms (https://www.applanix.com/). Two separate platforms were adopted to accommodate two separate sensor suites and their supporting hardware. Both flight sensor suites, one intended to encompass the VIS and NIR (VNIR) spectral regimes and the other the SWIR regime, were furnished by Headwall Photonics (http://www.headwallphotonics.com/). A Headwall Nano-Hyperspec® Hyperspectral Imaging Sensor, comprising 270 narrow bandwidth

spectral bands from 400-1000 nanometers (nm), 640 spatial bands, and a 7.4 micrometer pixel width, covered the VNIR regime. Likewise, for the SWIR regime, the Headwall Micro-Hyperspec SWIR® extended spectral reach from 950-2500 nm with 170 narrow bandwidth spectral bands. We opted for a spatial resolution, or ground sample distance (GSD), of 2.5 cm in our experimental design, thereby ensuring a high enough spatial resolution to capture even sub-leaf level spectral detail. UgCS ground station software was used for mission planning to achieve the required altitude and speed parameters for the sUAS platforms (https://www.ugcs.com/). It should be noted that there will be some level of image blur and optical point spread function effects, given the motion of the sUAS platform and its optical components. Consideration of image blur and point spread function effects becomes especially important when selecting a high spatial resolution (GSD) during flights. Such a small GSD would require increased integration times and introduce risk for notable image degradation, should the platform velocity not be adapted accordingly (Tico and Vehvilainen 2006).

One VNIR flight and one SWIR flight were flown over the same vineyard area, in successive fashion, between the times of 11h00-15h00 (EST) for each of the three flight campaign days. Flight paths were oriented parallel to vineyard rows and the sensor view was pointed in the nadir direction. The selection of flight locations was motivated by the geographical terrain features of the vineyard; we forecasted that terrain with a gradient in elevation might produce a natural range of vine moisture stress. Two separate blocks, or vineyard field partitions, in an east-west sloping vineyard were flown by the VNIR and SWIR platforms during each day of flight. Earlier examinations of these blocks had suggested disparity in the associated vine moisture status through the growing season.

The PMS Model 600 Pressure Chamber Instrument permitted the real-time traditional field measurement of ψ_{stem} during time of flight (https://www.pmsinstrument.com/). We selected various Cabernet Franc vine locations prior to flights, where mature and healthy leaves could be wrapped with aluminum foil bags for at least 45 minutes (Figure 4.4a), to allow for leaf equilibration and thus an integral measure of ψ_{stem} of the vine as a whole (Begg and Turner. 1970). Upon extraction from a vine, a given leaf was removed from the aluminum foil, placed inside of a thin plastic bag, and inserted into the pressure chamber instrument with xylem protruding out of a gland (Figure 4.4b). The resulting ψ_{stem} was given as a pressure in negative units of bars.

The individual leaves chosen in flight locations were placed within the aluminum foil bags ahead of flight execution to allow for sufficient equilibration time. Bright reference markers were inserted on the ground, contiguous to measured vine locations, to streamline subsequent image processing and analysis. Considering that ψ_{stem} is known to be highly variable with respect to time of day and atmospheric condition, ground measurement and associated flights were conducted in the most stable circumstances possible (Chone et al. 2001). Pressure chamber measurements were taken within 10 minutes of flight at each location. Altogether, we captured associated ψ_{stem} for 56 vines throughout all of the flights. The most significant water stress detected was -7.0 bars, which is considered to be a low level of stress (Möller et al. 2006).

Figure 4.3. Two separate multi-copter platforms were employed in our air campaign efforts. Both multi-copter designs exploited the modular DJI Matrice 600 flying platform. One of the multi-copters was equipped with a VNIR imaging sensor, while the other was equipped with a SWIR imaging sensor; both sensors boasted high spectral resolution – hyperspectral – sensors provided by Headwall Photonics (Izzo et al. 2019).

(a) (b)

Figure 4.4. A PMS Model 600 Pressure Chamber Instrument was used to capture the real-time traditional field measurement of ψ_{stem} during time of flight. Leaves were placed inside of aluminum bags before measurement to allow for assessment of integral plant water status (a) and then inserted into the pressure chamber instrument for measurement of ψ_{stem} (b) (Izzo et al. 2019)

4.4.3 Data preprocessing

The geospatial analytics software ENVI® (V5.5) was used during the initial processing of sUAS-captured spectral imagery. A mosaicking (stitching) procedure was required, since the Headwall pushbroom sensors aboard the sUAS platforms capture large areas by producing smaller individual frames. ENVI® hosts an available mosaicking function that allowed us to conjoin individual frames into larger mosaics with high precision, given the underlying georeferenced metadata. We needed to normalize the spectral image data to the reflectance space, from the original units of digital count; conversion to reflectance allowed direct comparison of all flights by removing atmospheric effects, i.e., by normalizing for varying illumination conditions. We used the well-known 2-Point Empirical Line Method (ELM) for our normalization needs, since it has been extensively demonstrated as a sufficiently stable and predictable means of calibrating spectral imagery (Roberts 1985). We used a Spectra Vista Corporation (SVC) HR-1024i spectroradiometer to record the spectral reflectance curves of at least two in-scene calibration panels of varying brightness levels (Figure 4.5), collected during the time of flights (https://www.spectravista.com/). A simple linear relationship between our digital count data and our SVC reflectance data for the in-scene panels facilitated a conversion of mosaicked imagery to the normalized reflectance space.

Next, an approach to separate or classify vine pixels from surrounding unwanted pixels was necessary, mainly because of the need to precisely associate flight data with particular vine

plots and pure foliage pixels. The extraction of vine pixels from the surrounding environment was critical, since the vine pixels in the sUAS imagery were those which we needed to associate with our in-field physiological measurements. A spectral classifier, called Spectral Angle Mapper (SAM), was utilized to identify the purest vine pixels against undesirable background pixels like soil, grass, and shadow. SAM is a classification technique that discerns spectral similarity based on an angular difference computation, given a reference spectral signature (Kuching 2007). We were able to extract a collection of vine pixels from field plots, by identifying a target vine pixel in the field plots and adjusting the allowable angular difference parameter as needed (Figure 4.6). The collection of SAM-classified pixels were averaged to obtain a single representative spectrum to associate with each field plot and associated ground measurement of ψ_{stem}. This procedure was completed for both the VNIR and SWIR data, such that we had resulting VNIR and SWIR spectral signatures that we could use alongside our traditional ψ_{stem} ground measurements.

Figure 4.5. We normalized all of our captured imagery to the reflectance space so that we could justifiably make direct comparison of all of our flight data across multiple days of flight. We placed in-scene calibration panels during all flights, and captured associated reflectance curves using an SVC spectrometer, to perform this normalization via the 2-point ELM (Izzo et al. 2019).

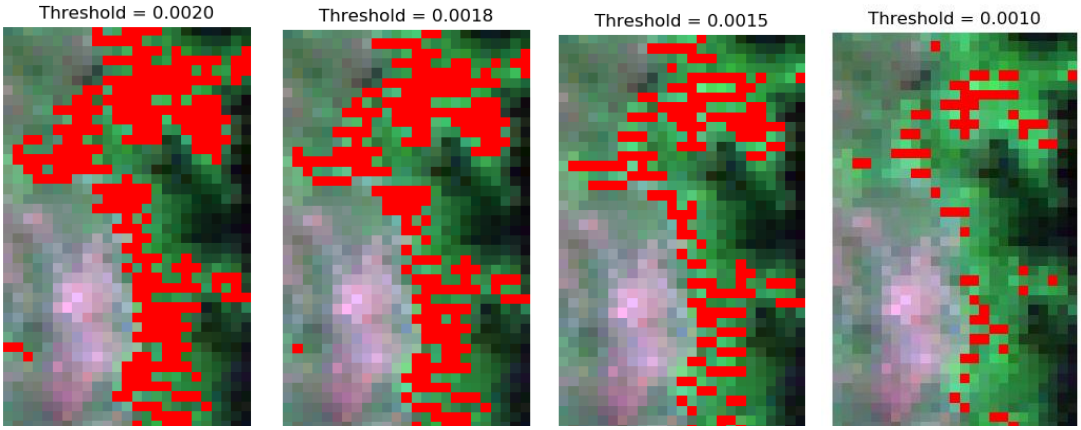

Figure 4.6. A spectral classification technique, called Spectral Angle Mapper (SAM), was used to separate vine pixels in the sUAS imagery data from unwanted pixel responses such as soil, grass, and shadow. An adjustment of the angular difference tuning parameter controls the level of strictness regarding spectral similarity. Note the varying classification results with increasing strictness in (a) through (d). For our purposes, we selected a strict threshold, i.e., 0.0010, to boost confidence in eliminating unwanted background or mixed pixels (Izzo et al. 2019).

Data analysis was carried out in Minitab® 19. We approached our analysis, with our objectives in mind, as three spectral ranges – VNIR only, SWIR only, and a mathematical conjoining of the two (Figure 4.7). Izzo et al. (2019) showed that the spectral data should be analyzed in its raw reflectance form, rather than after applying spectral smoothing, since there was the risk of removing potentially useful local absorption features with smoothing techniques. Due to low signal-to-noise ratio (SNR) in the region of 400-450 nm, these wavelength bands were discarded from consideration in our analyses (Izzo et al. 2019). Finally, given that the SWIR regime exhibits strong atmospheric water absorption features at approximately 1200 nm, 1400 nm, 1900 nm, and 2500 nm, these broad wavelength regions were removed to avoid impacts due to atmospheric interference; this enabled us to focus on strong atmospheric transmission windows for analysis (Clevers, Kooistra, and Schaepman 2010).

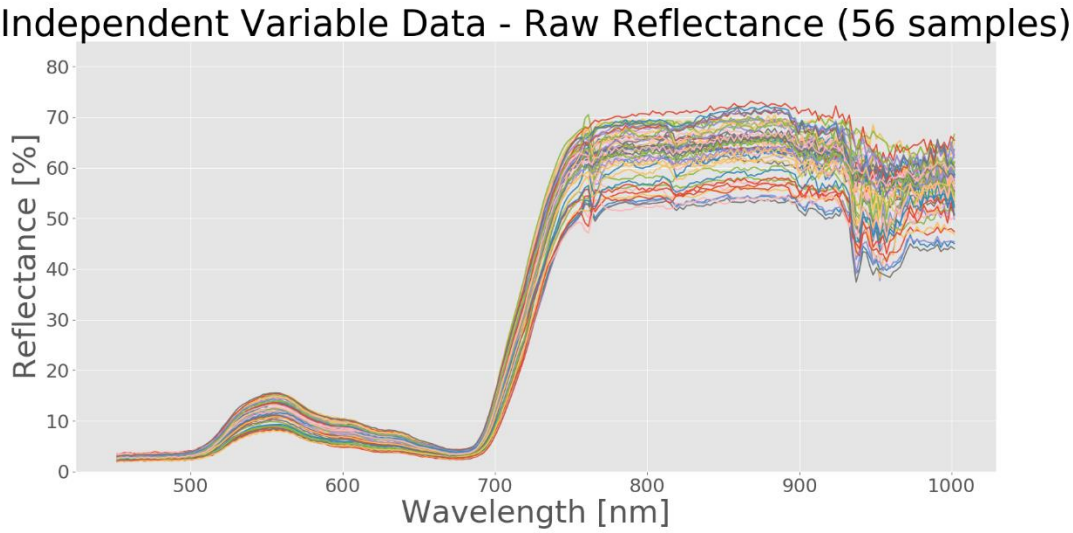

(a)

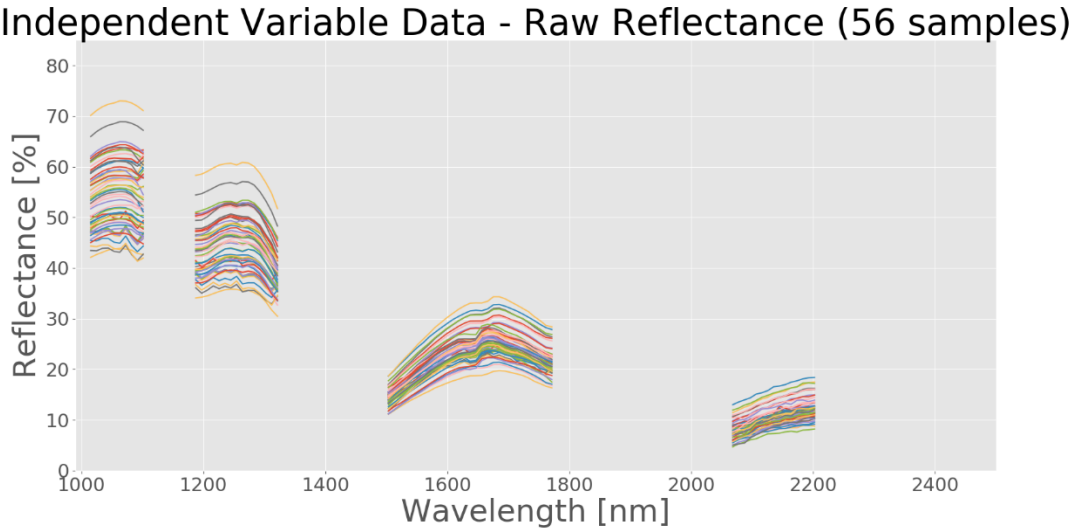

(b)

Figure 4.7. We produced 56 individual spectra for both the VNIR (a) and SWIR (b) regimes to be used in data modeling efforts. For the VNIR data, we omitted wavelengths from 400-450 nm due to low SNR. For the SWIR data, we removed the broad wavelength regions near the known water absorption features, while retaining the stronger transmission windows.

4.4.4 Modeling methods

The benefits of the oversampled spectral nature of hyperspectral data must be balanced with the obligatory practice of applying sound multivariate modeling and analysis techniques to

sort through such data; in short, we need to avoid the curse of data dimensionality and associated model over-fitting. In vegetation or environmental analyses, the intention is often to exploit the spectral power of hyperspectral data (narrow, contiguous bands across a broad wavelength range), while at the same time intelligently isolating the most pertinent spectral information through a robust data dimensionality scheme. It is understood that hyperspectral curves often exhibit correlated predictor variables, a phenomenon called multicollinearity, given the contiguous nature of the spectral data. Furthermore, in the current study, we had to contend with the additional challenge of having far more predictor variables than samples. Thus, there is the requirement to reduce dimensionality of hyperspectral data, while at the same time enabling examination of inevitably collinear and noisy data (Wold, Sjöström, and Eriksson 2001). In this work, we implemented two multivariate techniques with our data using Minitab® 19 – multiple linear regression (MLR) and partial least squares regression (PLSR) (Kokaly and Clark 1999; Wold, Sjöström, and Eriksson 2001).

In the case of MLR, a response variable is fit to a set of predictor variables by means of a simple linear equation. The response variable was ψ_{stem} in our case, while the predictor variables were selected wavelengths captured by the sUAS sensors. The stepwise case, on the other hand, is predicated on reduced predictor variables being iteratively chosen for addition or subtraction from a model, given some threshold or criterion which relates to explanatory power. We selected alpha significance levels to dictate the addition or subtraction of a given predictor. Data were also mean-centered by subtracting the mean and dividing by the standard deviation (Geladi and Kowalski 1986).

The MLR equation for a particular data sample can be written as

$$Y = \alpha_1 X_1 + \alpha_2 X_2 + \cdots + \alpha_p X_p + \beta + e$$

where α terms represent the coefficient values, X terms represent the predictors, β is an intercept value, and e is an error term (Kokaly and Clark 1999).

We also explored the application of PLSR (Wold, Sjöström, and Eriksson 2001), since the MLR method can often face difficulty when presented with a data set of significant multicollinearity or one with many more predictors than samples. PLSR is a statistical method, similar to principal components regression (PCR), in that both methods seek to minimize

covariance between predictors, but PLSR extends the concept further to also consider the responses by maximizing covariance between predictors and response (Geladi and Kowalski 1986). PLSR is implemented via matrix transformations applied on the response and predictor data sets. The predictor variables are transformed as

$$X = TP' + E = \sum t_h p'_h + E$$

where *X* represents the original predictor variables, *T* is the transformed latent variables, *P* contains the factor loadings, and *E* houses error terms (Geladi and Kowalski 1986).

The response data are correspondingly transformed as

$$Y = UQ' + F = \sum u_h q'_h + F$$

where the terms are analogous to those in the predictor data transformation.

In parameterizing our MLR data modeling, we selected alpha significance levels less than or equal to 0.10; our goal was to develop models that would contain fewer than 10 explanatory predictor variables (van Aardt et al. 2006). Parameterization of our PLSR models involved selection of latent variables with the lowest associated PRESS statistic (Geladi and Kowalski 1986).

4.4.4 Statistical analysis

We assessed the predictive capability of models using the coefficient of determination for calibration (R^2) and adjusted R^2. The adjusted R^2 metric allowed us to compare the performance of models with different numbers of predictors, thereby accounting for potential model over-fitting, or stated differently, being penalized for too many predictor variables. For this work, the proof of statistically significant trends proved more meaningful than predictive power, and were confirmed by comparing the alpha significance level and p-values; a model was taken to be statistically significant when the p-values were less than or equal to the alpha significance level. For all models, homoscedastic effects and normality of residuals were confirmed as acceptable (Bartlett 1937; Shapiro and Wilk 1965).

Multicollinearity effects were measured via the variance inflation factor (VIF) in the case of the MLR modeling efforts and given the potential adversarial effects of multicollinearity in

MLR. If the VIFs for any of the predictors in an MLR model exceeds 5, then it may be presumed that a significant level of collinearity exists and the use of PLSR to transform to uncorrelated components is further motivated (O'brien 2007). Finally, in the case of PLSR analyses, even though all of the predictors are used in the transformation to uncorrelated components, review of the standardized regression coefficients grants insight into the relative importance of a given predictor (Mehmood et al. 2012).

4.5 RESULTS

4.5.1 Stepwise multiple linear regression

MLR analyses were completed in Minitab® 19 for the VNIR, SWIR, and concatenated VNIR and SWIR data sets. Results are presented in Table 4.1. In order to discern statistical significance, the p-values for all terms in a model were verified as less than the selected alpha significance level for that given model. Moreover, normality of the residuals in each model were confirmed, as well as data homoscedastic or other similarly concerning effects (Figure 4.8).

There was a weak to moderate, but statistically significant, correlation in all cases tested. The VNIR data set exhibited the highest correlation, with an adjusted R^2 value of approximately 0.49. The concatenated VNIR-SWIR data did not translate into a distinct increased model performance. In fact, the selected wavelengths in the concatenated case were the same as those in the SWIR case and, as such, the performance metrics were the same.

Examination of the VIFs in the three MLR models presented showed that the VIF values exceeded 5 only in the case of VNIR data analysis, suggesting a level of collinearity between selected terms. This was not surprising, since the selected wavelength terms are close neighbors to each other on the spectral scale. The collinearity effects motivated the use of and are remedied by the PLSR analyses that followed.

Table 4.1. Summary of MLR analyses

Spectral dataset	**R^2**	**R^2 (adjusted)**	**Alpha (α) level**	**Selected wavelengths [nm]**
VNIR	0.55	0.49	0.075	474, 479, 499, 675, 690, 695
SWIR	0.34	0.31	0.10	1494, 2144
VNIR and SWIR	0.34	0.31	0.10	1494, 2144

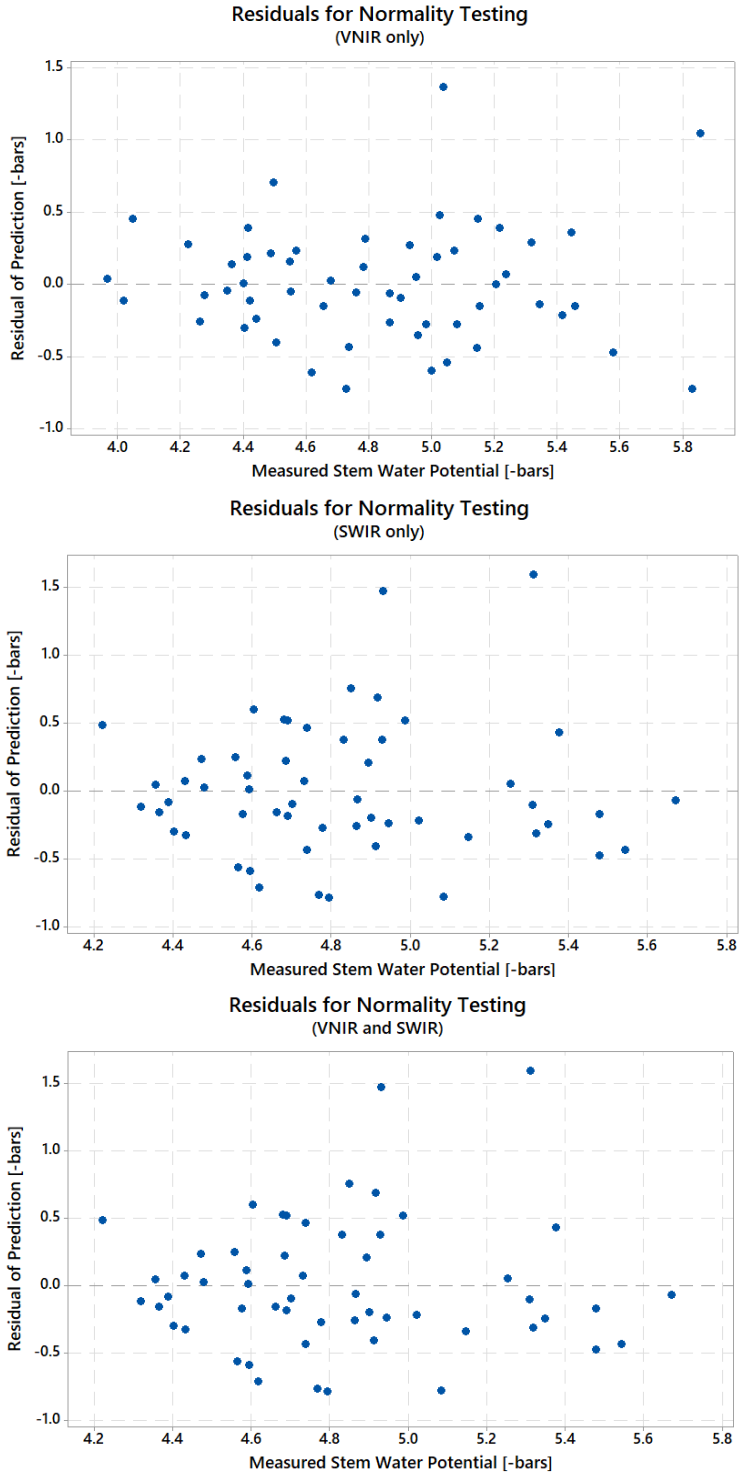

Figure 4.8. We confirmed the random distribution of residuals in our MLR models and noted the absence of homoscedastic effects in the plots for all analysis cases.

4.5.2 Partial least squares regression analysis

Analogous to MLR regression analyses, PLSR analyses also were completed in Minitab® 19 for the VNIR, SWIR, and concatenated VNIR and SWIR data sets. Results are presented in Table 4.2. The number of latent variables (LV), or uncorrelated components, for a given model were selected by retaining the number with the lowest associated PRESS statistic; the number of LVs retained was less than or equal to five in all cases. Again, there was a weak to moderate, but statistically significant, correlation in all cases tested. The standardized regression coefficients granted insight into the relative importance of terms in a given model (Figure 4.9). Terms, or wavelength bands, with higher standardized regression coefficient values may be taken as exhibiting greater importance in relating the response variable, or ψ_{stem} in our case.

Table 4.2. Summary of PLSR analyses

Spectral dataset	**R^2**	**R^2 (adjusted)**	**Number of LVs**
VNIR	0.39	0.34	4
SWIR	0.36	0.31	4
VNIR and SWIR	0.37	0.31	5

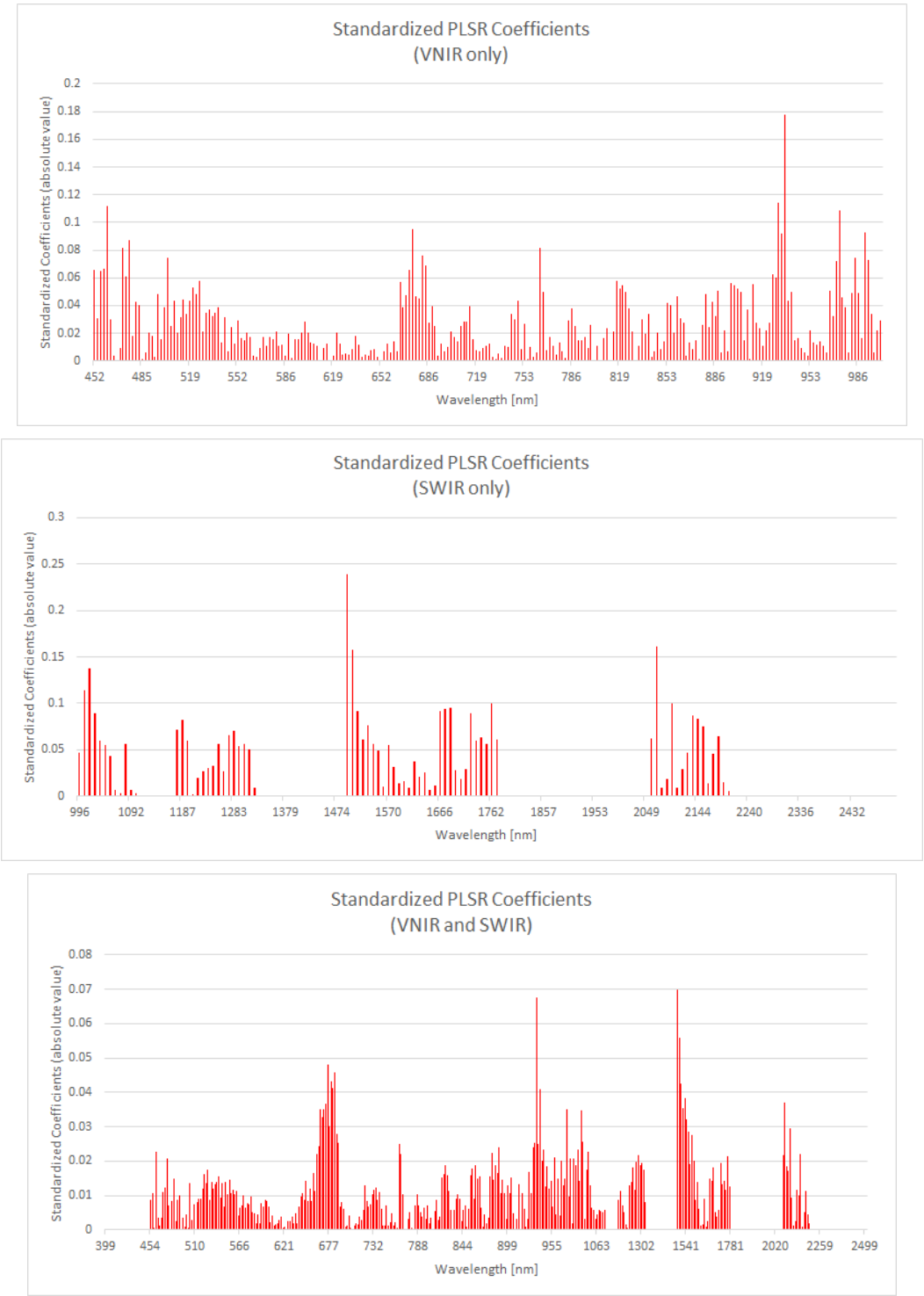

Figure 4.9. The standardized regression coefficients in PLSR granted insight into the relative importance of wavelength bands regarding the response variable. The x-axis represents wavelength in units of nanometers, and the y-axis represents a dimensionless regression coefficient. Relative peaks indicate wavelength bands which could be presumed to exhibit greater importance in the given model. The general trends in the coefficients seem to agree with the selected wavelengths in MLR models.

4.6 DISCUSSION

The MLR and PLSR outputs corroborated one another; in other words, the selected wavelengths in MLR models largely agreed with relative peaks in the standardized coefficient plots resulting from our PLSR efforts. This adds confidence in our data analysis via demonstrated stability across two separate multivariate regression techniques, i.e., we were able to discern select suggestive spectral trends and compare our findings to other studies. In fact, this between-method correspondence adds credence to the importance of selected wavelength regions, even though modeling performance arguably was not exceptional (high R^2 or adjusted-R^2 values). This is especially telling, given our observed narrow-range ψ_{stem} values. Next we will discuss the implications related to spectral-physiological linkages.

4.6.1 Carotenoid and chlorophyll concentration

It has been widely suggested that the ratio between carotenoid and chlorophyll a concentration is symptomatic of overall physiological sense of a plant (Penuelas, Baret, and Filella. 1995). Carotenoids absorb light (electro-magnetic radiation; EMR) in the blue region of the spectrum, while chlorophyll absorbs in the blue and red regions. In stressed or senescing leaves, the ratio of carotenoids to chlorophyll has been recognized to increase. For example, the normalized difference pigment index (NDPI) takes the normalized ratio between the reflectance values at the wavelengths 430 nm and 680 nm such that

$$NDPI = \frac{R_{680} - R_{430}}{R_{680} + R_{430}}$$

The NDPI indicator was later revised to a structure-independent pigment index (SIPI; (Josep Peñuelas and Filella 1998)) to minimize surface and structural effects, by using a reference NIR wavelength, such that

$$SIPI = \frac{R_{800} - R_{445}}{R_{800} - R_{680}}$$

Our results indicated importance of the wavelength bands in the regions of 470-500 nm and 670-700 nm, where chlorophyll and carotenoid absorption approximately occur, suggesting that the relative concentrations of chlorophyll and carotenoids could be deterministic with regard to grapevine moisture status, or the interactions between moisture stress and photosynthesis. Chlorophyll and carotenoid concentration have been shown as notable indicators of grapevine

moisture status in a number of studies (Zarco-Tejada et al. 2005; Rodríguez-Pérez et al. 2007; Zovko et al. 2019). Since the chlorophyll and carotenoid pigments are generally based on photosynthetic activity, rather than on any particular plant species, related implementations should be applicable across species. However, impactful spectral regions were not constrained to the photosynthetically active region (PAR) of EMR.

4.6.2 NIR and SWIR wavelengths

Our results pointed to the importance of a number of wavelength bands in the NIR and SWIR spectral regimes, known to be strongly related to plant moisture status – around 935 nm, 1494 nm, and 2144 nm. Wavelength bands situated in the NIR and SWIR regimes have been extensively used in the field for reliable indication of plant water (Behmann, Steinrücken, and Plümer 2014). One example is the Water Index (WI), defined as (J. Peñuelas et al. 1997)

$$WI = \frac{R_{900}}{R_{970}}$$

WI is widely used in the community for measurement of plant water concentration (PWC), and is predicated upon the minor, or weaker, water absorption feature located at around 970-980 nm. Further work addresses the sensitivity of the minor water absorption feature, and that it may shift to lower wavelengths between 930-950 nm under some conditions (J. Peñuelas et al. 1997). While it is possible that spectral characteristic at these lower wavelengths could be related to a water vapour absorption band in the same region, we contend that we applied sound atmospheric compensation techniques that would remove such interference in spectra (Gao and Goetz 1990). As such, our identified spectral feature at 935 nm is likely related to the second overtone in free O-H (Jin et al. 2017).

Reflectance deviations near 1500 nm also have been shown to be significantly correlated with change in leaf water content. The maximum difference water index (MDWI) compares maximum and minimum reflectance values at 1500 and 1750 nm to successfully relate leaf water content, and the region at 1500 nm has been used in novel spectral indices particularly for grapevine water stress assessment (Rapaport et al. 2015). It remained unclear precisely why the region near 2144 nm exhibited importance in our modeling efforts, however, the SWIR regime in general has been shown to be correlated with underlying plant moisture status (Josep Peñuelas and Filella 1998).

4.6.3 A comparison to previous studies

Baluja et al. (2012) reported that TCARI/OSAVI (a ratio between chlorophyll absorption and a soil-adjusted index) has a strong correlation with ψ_{stem} ($R^2 = 0.84$) in grapevine. Additionally, both Rodríguez-Pérez et al. (2007) and Zovko et al. (2019) found strong fits related to ψ_{stem} when leveraging the chlorophyll absorption in the PAR region. Our results corroborate the idea that the PAR region, and specifically the chlorophyll-a and chlorophyll-b absorption regions, are of critical importance for understanding grapevine moisture stress. Furthermore, in their continuum removal analysis efforts related to grapevine water, Rodríguez-Pérez et al. (2007) highlighted the utility of the maximum band depth associated with the water absorption feature at 970 nm ($R^2 = 0.509$) for vineyard moisture assessment. Zovko et al. (2019) also identified a number of applicable wavelengths in the SWIR regime, related to the intricate interactions of water, while particularly noting the O-H stretch in water and the longer wavelengths related to leaf water content. Again, our results corroborate this prior work, e.g., our indication that the minor water absorption feature at around 970 nm is critical to moisture assessment, while the longer wavelengths selected in our analyses overlap with those selected in the PLSR work of Zovko et al. (2019).

However, while we proved statistical significance in our modeling outcomes, the models' performance metrics were somewhat lower than those reported in previous studies. This is not surprising, given the very limited range of field-measured ψ_{stem} in our study. Our observed maximum of -7.0 bars for ψ_{stem}, arguably represents a very low level of moisture stress in grapevines. Baluja et al. (2012), in comparison, measured ψ_{stem} up to -14.0 bars and Zovko et al. (2019) applied controlled water treatments to experimental plots. We therefore contend that this study makes a contribution in i) corroborating that still significant modeling results can be achieved for a narrow moisture stress range, ii) full-range (400-2500 nm) sUAS imagery, collected at high spatial resolution (2.5 cm) contains enough signal to yield such significant models, and iii) that the relevant wavelengths regions/features remain consistent across analysis approaches and even studies/regions.

4.6.3 Future work recommended improvements

Access to experimental vineyard plots, which can be irrigation-controlled in future extension of this work or similar work, would be a distinct benefit. The application of controlled water treatments, such as those used by Zovko et al. (2019) would alleviate the problematic nature

of attempting to model a dependent variable with a limited response range. The coupling of the experimental design used in this study, with a full range of moisture stress values in grapevines, arguably would yield much stronger performance metrics than the ones presented here. The experimental outcomes also would stand to benefit from data collection under a single sUAS platform. Recall that we operated two contiguous flights during each of our flight days, collecting VNIR and SWIR spectral data separately, due to sUAS payload limitations. The use of a single platform, equipped to measure the full VNIR and SWIR spectral range, would eliminate the need to conduct separate flights for the VNIR and SWIR data acquisition, thereby ensuring image acquisition that is more coincident with field-measured ψ_{stem} values. Finally, as stated by Zovko et al. (2019), the precise separation between stress and senescence effects in plants requires a dataset that extends to the temporal dimension. The experimental design presented in this work arguably will perform successfully along the temporal dimension as well, due to its robust design, physiologically meaningful results, and consistent selection of specific spectral ranges.

4.7 CONCLUSIONS

The goal of this study was to fuse hyperspectral remote sensing, sUAS, and sound multivariate analysis techniques for the purposes of assessing grapevine moisture status. The specific objectives for this work included (1) an assessment of the overall potential of sUAS-based hyperspectral remote sensing for managing grapevine moisture status; (2) identifying the most pertinent spectral regions for discerning grapevine moisture status; and (3) interpreting findings for links to known plant physiological phenomena. We demonstrated statistically significant trends in our experiment, further qualifying the potential of utilizing downsampled hyperspectral data, collected via sUAS platforms, for the purposes of mapping, monitoring, and managing grapevine water status. There was indication that the chlorophyll and carotenoid absorption regions in the VIS could be useful in discerning grapevine water status. Furthermore, a number of wavelength regions in the NIR and SWIR - approximately located at 935 nm, 1494 nm, and 2144 nm - also were shown to be important in mapping vine moisture levels, and are worth further exploration. We showed that a consistent set of wavelength regions can be used to assess vineyard moisture status, even though our modeling results (R^2 and adjusted R^2 values) were less than stellar, but still significant. For example, our multiple linear regression efforts yielded R^2 values between 0.34 and

0.55 and our partial least squares regression yielded R^2 values between 0.36 and 0.39. This somewhat poorer model performance was attributed to the narrow range of field-measured ψ_{stem} values, i.e., the higher-than-typical seasonal rainfall resulted in less variability in ψ_{stem} than we had hoped for. As such this work was limited in the fact that we did not have access to vineyard plots which could be experimentally controlled for conditions under test, and we therefore recommend that future work ensure experimental control for a full, larger range of moisture stress in the vines. Nonetheless, the application of hyperspectral imaging and sUAS platforms in grapevine water management remains lucrative and additional work to further operationalize these systems for precision viticulture would be valuable to the larger vineyard agricultural community.

Chapter 5

Summary

5.1 SUMMARY

Chapter 1 of this thesis provides the context for studying grapevine moisture by means of remote sensing technologies. Current methods of grapevine moisture management are explained, and the benefits associated with operationalizing remote sensing technologies are presented and justified. Our overarching objective was to assess the utility of sUAS-based (hyper-) spectral indicators for assessing limited variation in vineyard moisture status, toward establishing potential operational solutions. The specific objectives of the thesis were also presented, namely to 1) Evaluate a sound data processing chain to relate hyperspectral data and field (moisture) physiological indicators for a commercial rainfed vineyard, 2) Assess the overall potential of sUAS-based hyperspectral remote sensing for managing grapevine moisture status, 3) Identify pertinent spectral indicators in the VNIR spectral regime for discerning grapevine moisture status, 4) Identify pertinent spectral indicators in the SWIR spectral regime for discerning grapevine moisture status, and 5) Publish research findings as a comprehensive technical manuscript in an applicable precision agriculture journal for targeted outreach. Furthermore, the scientific contributions of the work are clearly stated.

Chapter 2 provides a review of some of the seminal work done in relation to remote sensing for grapevine moisture to provide a brief background to set up and further motivate Chapters 3 and 4. Since Chapters 3 and 4 were written as research papers, the background provided in those chapters was written in a targeted and specific format. Thus, Chapter 2 provides deeper insights into the literature review that was not directly stated in the primary Chapters 3 and 4.

Chapter 3 represented a paper that was presented and published in the Autonomous Air and Ground Sensing Systems for Agricultural Optimization and Phenotyping session of the SPIE Defense and Commercial Sensing Conference proceedings, April 2019 (Izzo et al. 2019). It details initial modeling and data analysis efforts for the VNIR data that we had collected. These initial efforts aided in developing a sound experimental design to motivate a more comprehensive and exhaustive analysis and provided some initial confidence in the overall potential of sUAS-based hyperspectral remote sensing for managing grapevine moisture status.

Chapter 4 provided a more exhaustive and robust analysis and acts as an extension to the work presented in Chapter 3. The analysis includes the SWIR data collected in the field, for a full range (400-2500 nm) study, and aims to establish links to plant physiological phenomena. By correlating traditional field measurements of stem water potential (ψ_{stem}) and sUAS-based hyperspectral data, it was demonstrated that statistically significant trends can be shown even given a narrow range of moisture stress in grapevine. The work suggested that the chlorophyll and carotenoid absorption regions in the VNIR, as well as several SWIR water band regions should be further explored in related works. The chapter is written with the intent to publish in an applicable peer-reviewed journal in the 2019 timeframe.

5.2 CONCLUSIONS

Since grapes are one of the most economically-important agricultural crops in the world, there is a significant interest in maintaining and increasing the associated quality of grapes and resulting wine product for economic and cultural reasons. The presence of a mild moisture deficit in grapevines prompts a reduction in shoot growth, berry weight, and yield, all of which are factors that collectively serve to inflate berry anthocyanin and tannin levels and, as such, perceived quality (Cornelis Van Leeuwen et al. 2009). Controlled deficit irrigation emerged as one method to induce mild moisture deficit stress in grapevines, and has been demonstrated to yield improved berry

quality, while maintaining operationally acceptable yields (Chaves et al. 2007). Deficit irrigation, or partial irrigation, reduces vine vigour and shoot growth in a controlled manner that shifts plant metabolic processes to induce improved fruit quality (Matthews and Anderson 1989). Similarly, in vineyards where deficit irrigation techniques cannot be realized, the knowledge of vine water status may dictate selective harvesting practices, giving way to optimized quality and yield. Selective harvesting can be successfully implemented in both small quantity producing wineries, as well as those with large volume and flexible infrastructure (Bramley et al. 2005).

Traditionally, management of vine moisture status has been facilitated by direct in-field measurement of sensitive physiological indicators. The in-field direct measurement of ψ_{stem} with a manual pressure chamber, while proven valid for grapevine water status measurement (Chone et al. 2001), is challenging for large, commercial vineyards. While strides have been made in numerous vineyard settings to operationally respond to in-field measures of vine moisture status, accurate measurements often require an inordinate amount of time and labor, and progress in operational application remains gradual (Rodríguez-Pérez et al. 2007). It is in this context that remote sensing technology has become an increasingly common tool to remotely probe for plant physiological indicators, like plant moisture status, via observations of the unique electromagnetic spectral response related to plant moisture regimes. The potential superiority of non-destructive remote sensing techniques, for these purposes, lies in the cost-effective, exhaustive ("wall-to-wall"), and objective nature of application (Govender et al. 2009).

Our research fused hyperspectral remote sensing, sUAS, and sound multivariate analysis techniques for the purposes of assessing grapevine water status. We conducted full airborne (sUAS) and ground (field truth) campaigns and analyzed our data using sound modeling techniques, all in order to present trends and conclusions to inform future efforts. There still is a need to further evaluate sUAS-based, high spatial resolution, and especially hyperspectral imagery for different geographic regions, thereby validating past efforts for different regions and grape varieties. Most of the prior work utilizes data that were collected in situ via spectroradiometers. For those studies that did include a sUAS platform, many did not evaluate the optical domain, and some did not correlate with reliable physiological indicators. We therefore attempted to bridge that gap to some extent in this work, fusing hyperspectral remote sensing, sUAS, and sound multivariate analysis techniques for the purposes of assessing grapevine water status.

Our first cursory analysis focused only on VNIR data that we had collected during our field campaign efforts. We collected high-spatial resolution imagery (2.5 cm GSD) over 3 flight days via an sUAS platform, and ψ_{stem} ground measurements in which to correlate with via a pressure chamber, captured coincident to the flights. Our first analysis (Chapter 3) was most significant in developing and evaluating a sound data processing chain for our study. We used a Spectral Angle Mapping classifier to enable the targeting of pure (sunlit) vine canopy with vertically trained shoots and significant shadowing. We decided to use the partial least squares-regression (PLS-R) modeling method to correlate our hyperspectral imagery with measured field water status and applied a wavelength band selection scheme to detect important wavelengths. We evaluated spectral smoothing and band reduction approaches, given signal-to-noise ratio (SNR) concerns. Our regression results indicated that unsmoothed curves, with the range of wavelength bands from 450-1000 nm, provided the highest model performance with $R^2 = 0.68$ for cross-validation. There may have been some issues of overfitting during this first cursory analysis, which were remedied by removing the wavelength band selection scheme in the more comprehensive manuscript presented in Chapter 4.

Chapter 4 further expands upon the results of Chapter 3 by including the SWIR data collected in the field and discerning links to plant physiological phenomena. We correlated our hyperspectral data with a limited stress range (wet growing season) of traditional measurements for ψ_{stem} using multiple linear regression (R^2 between 0.34 and 0.55) and partial least squares regression (R^2 between 0.36 and 0.39). We demonstrated statistically significant trends in our experiment, further qualifying the potential of hyperspectral data, collected via sUAS, for the purposes of grapevine water management. There was indication that the chlorophyll and carotenoid absorption regions in the VNIR, while several SWIR water band regions warrant further exploration.

This work had several significant contributions relative to the perceived research gap in the current body of work. We provided evidence that correlation can be established between field ψ_{stem} and hyperspectral data of grapevine, even given a relatively narrow-range of ψ_{stem} response. As more studies utilize sUAS platforms to collect data for similar studies, we demonstrated sound data processing techniques that might be considered in future works. Furthermore, we showed statistically-significant trends when relating grapevine ψ_{stem} to downsampled hyperspectral data collected across the VNIR and SWIR spectral regimes (400-2500 nm), that future work may

evaluate or validate. Specifically, we suggested the importance of understanding the chlorophyll and carotenoid absorption regions for grapevine, we confirmed the NIR minor water absorption feature (970 nm) as being a useful indicator for understanding grapevine moisture, as already indicated by a number of established spectral indices in the literature, and highlighted select longer wavelength regions in the SWIR that might be considered in grapevine moisture studies.

5.3 FUTURE WORK AND IMPROVEMENTS

As we progressed through the research presented in this thesis, we learned and noted improvements or changes in experimental design that could benefit future, related work. These changes/improvements include the following:

- Stem water potential (ψ_{stem}) is a sensitive physiological indicator that is known to change throughout the day, given atmospheric/environmental conditions present at the study site. In our work, we were required to fly two separate flights during data collection days (one VNIR and one SWIR) due to sUAS payload limitations. In other words, it may be that our VNIR and SWIR data were collected under slightly different conditions, even though the flights were contiguous in time and ψ_{stem} field measurements were coincident to image acquisition. As such, it would be recommended that future work aim to use a single platform, equipped to measure the full VNIR and SWIR spectral range, thereby ensuring image acquisition that is even more coincident with field-measured ψ_{stem} values.
- It has been shown in many previous studies that predictive models tend to be more robust if backed up by many data samples, i.e., much greater than the 56 field data samples we had at our disposal for this research effort. Our small number of field samples was primarily due to the time and expertise involved in accurately measuring ψ_{stem} with a pressure chamber; specifically, we had one subject matter expert to capture these measurements. Future related work might consider planning to have multiple pressure chambers and subject matter experts available for field measurements, to ensure a greater number of data samples to model.
- We had the unfortunate incidence, for research purposes, of significant rainfall during

a growing season in which we were hoping to capture a significant range/variability for moisture stress in grapevine. We therefore had no option but to accept a limited range of moisture stress with which to model field-measured ψ_{stem}. We were still able to show statistically significant trends, but it would be recommended that future efforts implement water treatments in experimental plots to ensure a wider range of stress. This may require finding an experimental vineyard or a commercial vineyard willing to facilitate an experimental area for such a study.

- We built our models in this research given a single field parameter to correlate with, namely stem water potential (ψ_{stem}). Other studies related to additional field parameters, which may be helpful for understanding moisture stress in grapevines; one such a parameter example is stomatal conductance (g).
- While we had AeroPoints™ placed in the field in order to increase accuracy during mosaicking efforts, in addition to the onboard GPS, they were not used as part of the data processing chain in this work. The AeroPoints™ would help with any mosaicking error, e.g., you could identify an AeroPoint™ in a mosaic and use that center point to improve registration accuracy.
    - In order to review how the lack of AeroPoints affected image registration, we used ENVI to evaluate image registration between the two spectrometers, for one block during one of the collect days; RMS error in ENVI was reported as ~15 pixels (about what we would expect with the onboard GPS). This did not impact our work, since we manually located the field plots in the image data, based on the orange plate markers that we had placed out in the field. However, if a study required automatic location of field plots via image registration efforts, they should expect an error ~15 pixels and therefore should consider the integration of precise GPS data from the AeroPoints™.
- The process of conjoining VNIR and SWIR spectral data, collected on two separate sUAS platforms, could have been more rigorous. In our work, we conjoined or stacked the VNIR and SWIR spectral curves from two independent sources. There are more complex methods that may be used to address the potential error introduced by differences in time between flights. Future studies should aim to develop a more robust

method of conjoining independent spectral curves, given the potential separation in time between sUAS flights, and with recognition that plant physiological measurements can change rather rapidly.

Appendix A

A.1 Fox Run Vineyards Map

Figure A.1.1. Fox Run offers a complex terroir that made it an attractive choice for our study. The terrain has a significant gradient in elevation, from 470 to 700 feet, in relation to distance from lake edge. Furthermore, the soils host a complex combination of sandy loam and gravelly clay across the extent of the vineyard.

Appendix B

A.2 Data Analysis Raw Outputs

Regression Analysis: Ref SWP versus 451.996002, ... 6975, 1001.809998

Stepwise Selection of Terms

α to enter = 0.075, α to remove = 0.075

Analysis of Variance

Source	DF	Adj SS	Adj MS	F-Value	P-Value
Regression	6	10.5257	1.7543	9.81	0.000
474.256012	1	2.9869	2.9869	16.70	0.000
478.708008	1	2.6335	2.6335	14.73	0.000
498.742004	1	0.7737	0.7737	4.33	0.043
674.593994	1	3.9194	3.9194	21.92	0.000
690.176025	1	1.5899	1.5899	8.89	0.004
694.627991	1	0.6217	0.6217	3.48	0.068
Error	49	8.7627	0.1788		
Total	55	19.2884			

Model Summary

S	R-sq	R-sq(adj)	R-sq(pred)
0.422883	54.57%	49.01%	38.72%

Coded Coefficients

Term	Coef	SE Coef	T-Value	P-Value	VIF
Constant	4.8196	0.0565	85.29	0.000	
474.256012	-2.354	0.576	-4.09	0.000	102.02
478.708008	1.460	0.380	3.84	0.000	44.51
498.742004	1.101	0.529	2.08	0.043	86.17
674.593994	-1.169	0.250	-4.68	0.000	19.16
690.176025	1.517	0.509	2.98	0.004	79.59
694.627991	-0.668	0.358	-1.86	0.068	39.45

Regression Equation in Uncoded Units

Ref SWP = 5.862 - 5.05 474.256012 + 2.870 478.708008 + 2.14 498.742004 - 2.069 674.593994
+ 1.595 690.176025 - 0.421 694.627991

Figure A.2.1. VNIR stepwise results from Minitab, $R^2 = 0.55$

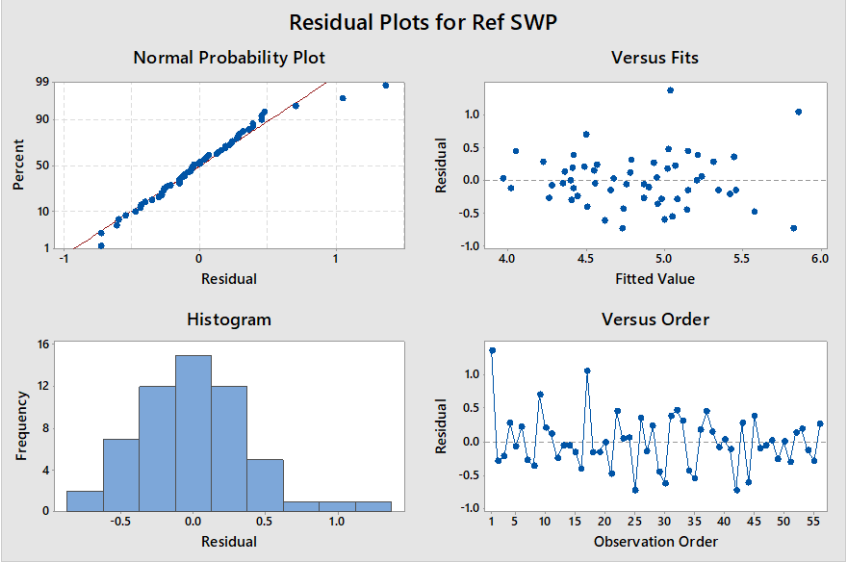

Figure A.2.2 (continued) VNIR stepwise plots from Minitab; the residual plots confirm random distribution; the detailed stepwise procedure shows the process of adding variables into the model and associated R^2 performance

	Step 1		**Step 2**		**Step 3**		**Step 4**	
	Coef	P-value	Coef	P-value	Coef	P-value	Coef	P-value
Constant	4.8196		4.8196		4.8196		4.8196	
675 nm	-0.1539	0.053	-1.238	0.000	-1.327	0.000	-1.301	0.000
690 nm			1.108	0.000	0.849	0.004	0.739	0.008
497 nm					0.381	0.067	1.350	0.001
474 nm							-0.908	0.004
478 nm								
499 nm								
695 nm								
R^2 (adj)	0.05		0.29		0.32		0.41	
	Step 5		**Step 6**		**Step 7**		**Step 8**	
	Coef	P-value	Coef	P-value	Coef	P-value	Coef	P-value
Constant	4.8196		4.8196		4.8196		4.8196	
675 nm	-1.271	0.000	-1.238	0.000	-1.042	0.000	-1.169	0.000
690 nm	0.907	0.002	1.080	0.000	0.734	0.016	1.517	0.004
497 nm	0.677	0.181						
474 nm	-1.484	0.001	-1.512	0.001	-2.359	0.000	-2.354	0.000
478 nm	1.066	0.056	1.574	0.000	1.496	0.000	1.460	0.000
499 nm					1.073	0.053	1.101	0.043
695 nm							-0.668	0.068
R^2 (adj)	0.44		0.44		0.46		0.49	

Figure A.2.2 (continued) VNIR stepwise plots from Minitab; the residual plots confirm random distribution; the detailed stepwise procedure shows the process of adding variables into the model and associated R^2 performance

PLS Regression: Ref SWP versus 451.996002, 454.221985, ... 01.809998

Method

Cross-validation	Leave-one-out
Components to evaluate	Set
Number of components evaluated	10
Number of components selected	4

Analysis of Variance for Ref SWP

Source	DF	SS	MS	F	P
Regression	4	7.5369	1.88422	8.18	0.000
Residual Error	51	11.7515	0.23042		
Total	55	19.2884			

Model Selection and Validation for Ref SWP

Components	X Variance	Error	R-Sq	PRESS	R-Sq (pred)
1	0.714520	18.9020	0.020035	20.2982	0.000000
2	0.896245	17.5524	0.090002	20.4474	0.000000
3	0.935953	14.1441	0.266705	19.1838	0.005422
4	0.958337	11.7515	0.390748	15.2414	0.209813
5		9.8200	0.490888	15.7453	0.183690
6		8.6028	0.553993	16.0514	0.167819
7		7.4904	0.611662	17.9881	0.067413
8		6.9516	0.639594	18.4520	0.043365
9		3.7785	0.804104	20.7774	0.000000
10		2.4265	0.874201	20.4081	0.000000

Figure A.2.3. VNIR PLS results from Minitab, $R^2 = 0.39$

Regression Analysis: Ref SWP versus 995.789978, ... 0098, 2201.919922

Stepwise Selection of Terms

α to enter = 0.1, α to remove = 0.1

Analysis of Variance

Source	DF	Adj SS	Adj MS	F-Value	P-Value
Regression	2	6.494	3.2472	13.45	0.000
1493.560059	1	5.893	5.8931	24.41	0.000
2144.48999	1	2.181	2.1813	9.04	0.004
Error	53	12.794	0.2414		
Total	55	19.288			

Model Summary

S	R-sq	R-sq(adj)	R-sq(pred)
0.491322	33.67%	31.17%	25.43%

Coded Coefficients

Term	Coef	SE Coef	T-Value	P-Value	VIF
Constant	4.8196	0.0657	73.41	0.000	
1493.560059	0.546	0.110	4.94	0.000	2.78
2144.48999	-0.332	0.110	-3.01	0.004	2.78

Regression Equation in Uncoded Units

Ref SWP = 3.081 + 0.2815 1493.560059 - 0.1723 2144.48999

Figure A.2.4. SWIR stepwise results from Minitab, $R^2 = 0.34$

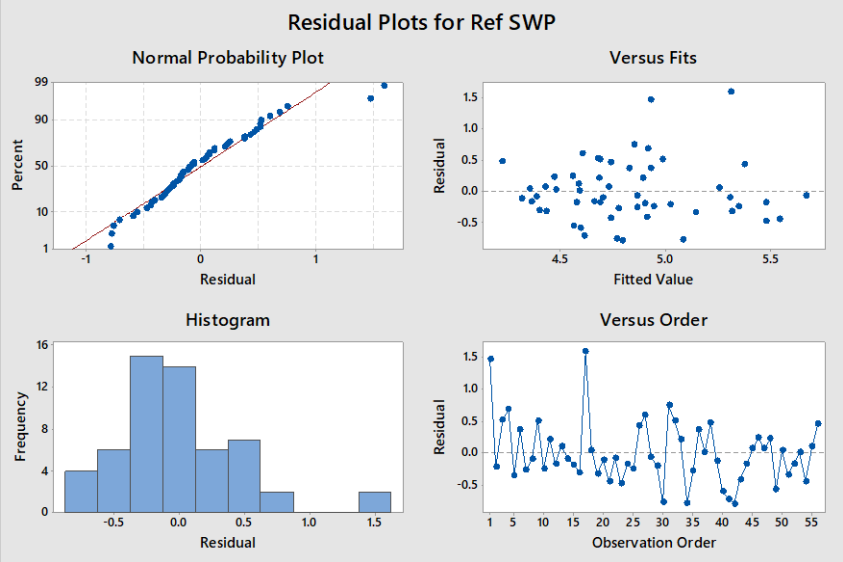

	Step 1		**Step 2**	
	Coef	P-value	Coef	P-value
Constant	4.8196		4.8196	
1494 nm	0.2800	0.000	0.546	0.000
2144 nm			-0.332	0.004
R^2 (adj)	0.21		0.31	

Figure A.2.5. SWIR stepwise plots from Minitab; the residual plots confirm random distribution; the detailed stepwise procedure shows the process of adding variables into the model and associated R^2 performance

PLS Regression: Ref SWP versus 995.789978, ... 2.350098, 2201.919922

Method

Cross-validation	Leave-one-out
Components to evaluate	Set
Number of components evaluated	10
Number of components selected	4

Analysis of Variance for Ref SWP

Source	DF	SS	MS	F	P
Regression	4	6.8811	1.72029	7.07	0.000
Residual Error	51	12.4072	0.24328		
Total	55	19.2884			

Model Selection and Validation for Ref SWP

Components	X Variance	Error	R-Sq	PRESS	R-Sq (pred)
1	0.734132	17.8253	0.075851	19.1585	0.006736
2	0.949541	15.9964	0.170673	18.0035	0.066615
3	0.986966	13.5395	0.298050	15.9682	0.172132
4	0.994417	12.4072	0.356751	15.4255	0.200270
5		11.3530	0.411407	16.0064	0.170152
6		11.0648	0.426352	16.1033	0.165129
7		10.3035	0.465821	18.3919	0.046481
8		9.3266	0.516463	21.8094	0.000000
9		8.3013	0.569620	24.8553	0.000000
10		7.3578	0.618536	27.8682	0.000000

Figure A.2.6. SWIR PLS results from Minitab, $R^2 = 0.36$

Regression Analysis: Ref SWP versus 451.996002, ... 0098, 2201.919922

Stepwise Selection of Terms

α to enter = 0.1, α to remove = 0.1

Analysis of Variance

Source	DF	Adj SS	Adj MS	F-Value	P-Value
Regression	2	6.494	3.2472	13.45	0.000
1493.560059	1	5.893	5.8931	24.41	0.000
2144.48999	1	2.181	2.1813	9.04	0.004
Error	53	12.794	0.2414		
Total	55	19.288			

Model Summary

S	R-sq	R-sq(adj)	R-sq(pred)
0.491322	33.67%	31.17%	25.43%

Coded Coefficients

Term	Coef	SE Coef	T-Value	P-Value	VIF
Constant	4.8196	0.0657	73.41	0.000	
1493.560059	0.546	0.110	4.94	0.000	2.78
2144.48999	-0.332	0.110	-3.01	0.004	2.78

Regression Equation in Uncoded Units

Ref SWP = 3.081 + 0.2815 1493.560059 - 0.1723 2144.48999

Residual Plots for Ref SWP

Figure A.2.7. VNIR-SWIR stepwise results from Minitab, $R^2 = 0.34$

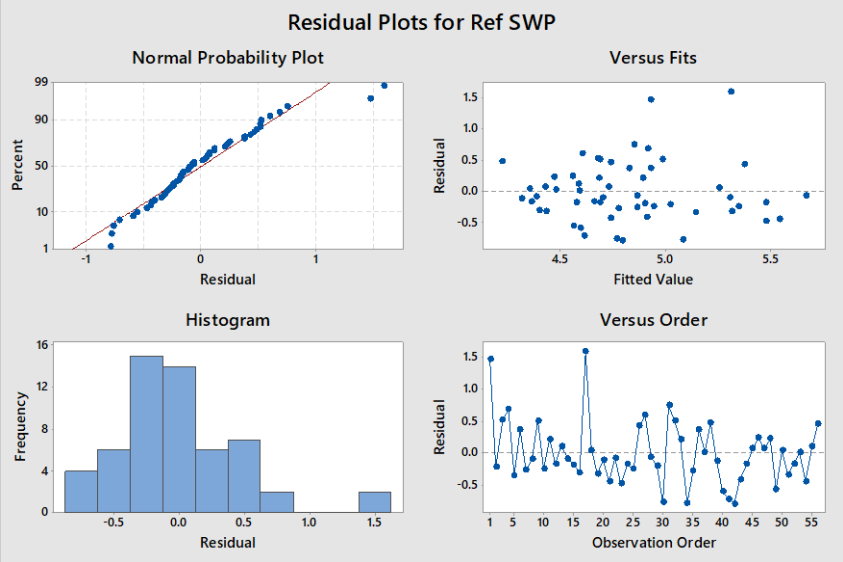

	Step 1		**Step 2**	
	Coef	P-value	Coef	P-value
Constant	4.8196		4.8196	
1494 nm	0.2800	0.000	0.546	0.000
2144 nm			-0.332	0.004
R^2 (adj)	0.21		0.31	

Figure A.2.8. VNIR-SWIR stepwise plots from Minitab; the residual plots confirm random distribution the detailed stepwise procedure shows the process of adding variables into the model and associated R^2 performance

PLS Regression: Ref SWP versus 451.996002, 454.221985, ... 201.919922

Method

Cross-validation	Leave-one-out
Components to evaluate	Set
Number of components evaluated	10
Number of components selected	5

Analysis of Variance for Ref SWP

Source	DF	SS	MS	F	P
Regression	5	7.2169	1.44338	5.98	0.000
Residual Error	50	12.0715	0.24143		
Total	55	19.2884			

Model Selection and Validation for Ref SWP

Components	X Variance	Error	R-Sq	PRESS	R-Sq (pred)
1	0.342178	17.3994	0.097936	20.7916	0.000000
2	0.734372	16.1301	0.163740	20.4491	0.000000
3	0.828098	13.8659	0.281129	18.2326	0.054735
4	0.937266	13.1324	0.319156	17.6274	0.086116
5	0.960210	12.0715	0.374157	16.8965	0.124005
6		11.1197	0.423504	16.9551	0.120971
7		9.4437	0.510394	17.0798	0.114506
8		8.8125	0.543119	17.6637	0.084232
9		7.5316	0.609526	19.9653	0.000000
10		6.5537	0.660224	23.1770	0.000000

Figure A.2.9. VNIR-SWIR PLS results from Minitab, $R^2 = 0.37$

Bibliography

Aardt, Jan van, J Holmgren, M Nilsson, and H Olsson. 2006. “Forest Volume and Biomass Estimation Using Small-Footprint Lidar-Distributional Parameters.” *Forest Science* 49 (3): 419–28. http://www.ingentaconnect.com/content/saf/fs/2006/00000052/00000006/art00003.

Ač, Alexander, Zbyněk Malenovský, Julie Olejníčková, Alexander Gallé, Uwe Rascher, and Gina Mohammed. 2015. “Meta-Analysis Assessing Potential of Steady-State Chlorophyll Fluorescence for Remote Sensing Detection of Plant Water, Temperature and Nitrogen Stress.” *Remote Sensing of Environment* 168: 420–36.

Acevedo-Opazo, C., Bruno Tisseyre, Serge Guillaume, and H. Ojeda. 2008. “The Potential of High Spatial Resolution Information to Define Within-Vineyard Zones Related to Vine Water Status.” *Precision Agriculture* 9 (5): 285–302.

Andersen, Charlotte Møller, and Rasmus Bro. 2010. “Variable Selection in Regression—a Tutorial.” *Journal of Chemometrics* 24 (11–12): 728–37.

Ballester, Carlos, P. J. Zarco-Tejada, E. Nicolás, J. J. Alarcón, E. Fereres, Diego S. Intrigliolo, and V. J. P. A. Gonzalez-Dugo. 2018. “Evaluating the Performance of Xanthophyll, Chlorophyll and Structure-Sensitive Spectral Indices to Detect Water Stress in Five Fruit Tree Species.” *Precision Agriculture* 19 (1): 178–93.

Baluja, Javier, Maria P. Diago, Pedro Balda, Roberto Zorer, Franco Meggio, Fermin Morales, and Javier Tardaguila. 2012. “Assessment of Vineyard Water Status Variability by Thermal and Multispectral Imagery Using an Unmanned Aerial Vehicle (UAV).” *Irrigation Science* 30 (6): 511–22.

Bartlett, Maurice Stevenson. 1937. “Properties of Sufficiency and Statistical Tests.” *Proceedings of the Royal Society of London Series A-Mathematical and Physical Sciences* 160 (901): 268–82.

Bastiaanssen, Wim GM, David J. Molden, and Ian W. Makin. 2000. “Remote Sensing for Irrigated Agriculture: Examples from Research and Possible Applications.” *Agricultural Water Management* 46 (2): 137–55.

Bayer. 2019. “Grapevine/Grape.” 2019. https://www.cropscience.bayer.com/en/crop-compendium/crops/grapevine-grape.

Begg, John E., and Neil C. Turner. 1970. “Water Potential Gradients in Field Tobacco.” *Plant Physiology* 46 (2): 343–46.

Behmann, Jan, Jörg Steinrücken, and Lutz Plümer. 2014. “Detection of Early Plant Stress Responses in Hyperspectral Images.” *ISPRS Journal of Photogrammetry and Remote Sensing* 93: 98–111.

Bei, Roberta De, Daniel Cozzolino, Wendy Sullivan, W. Cynkar, Sigfredo Fuentes, R. Dambergs, J. Pech, and Stephen Tyerman. 2011. “Non-destructive Measurement of Grapevine Water Potential Using near Infrared Spectroscopy.” *Australian Journal of Grape*

and Wine Research 17 (1): 62–71.

Bellvert, Joaquim, Pablo J. Zarco-Tejada, Joan Girona, and E. J. P. A. Fereres. 2014. "Mapping Crop Water Stress Index in a 'Pinot-Noir'Vineyard: Comparing Ground Measurements with Thermal Remote Sensing Imagery from an Unmanned Aerial Vehicle." *Precision Agriculture* 15 (4): 361–76.

Bramley, R. G. V., A. P. B. Proffitt, C. J. Hinze, B. Pearse, and R. P. Hamilton. 2005. "Generating Benefits from Precision Viticulture through Selective Harvesting." *Precision Agriculture* 5: 891–98.

Buitrago, Maria F., Thomas A. Groen, Christoph A. Hecker, and Andrew K. Skidmore. 2016. "Changes in Thermal Infrared Spectra of Plants Caused by Temperature and Water Stress." *ISPRS Journal of Photogrammetry and Remote Sensing* 111: 22–31.

Caruso, Giovanni, Letizia Tozzini, Giovanni Rallo, Jacopo Primicerio, Marco Moriondo, G. Palai, and Riccardo Gucci. 2017. "Estimating Biophysical and Geometrical Parameters of Grapevine Canopies ('Sangiovese') by an Unmanned Aerial Vehicle (UAV) and VIS-NIR Cameras." *Vitis* 56 (2): 63–70.

Chaves, Maria Manuela, Tiago P. Santos, CR de Souza, M. F. Ortuño, M. L. Rodrigues, C. M. Lopes, J. P. Maroco, and João Santos Pereira. 2007. "Deficit Irrigation in Grapevine Improves Water-use Efficiency While Controlling Vigour and Production Quality." *Annals of Applied Biology* 150 (2): 237–52.

Chone, Xavier, Cornelis Van Leeuwen, Denis Dubourdieu, and Jean Pierre Gaudillère. 2001. "Stem Water Potential Is a Sensitive Indicator of Grapevine Water Status." *Annals of Botany* 87 (4): 477–83.

Clevers, Jan GPW, Lammert Kooistra, and Michael E. Schaepman. 2010. "Estimating Canopy Water Content Using Hyperspectral Remote Sensing Data." *International Journal of Applied Earth Observation and Geoinformation* 12 (2): 119–25.

Damm, A., E. Paul-Limoges, E. Haghighi, C. Simmer, F. Morsdorf, F. D. Schneider, C. van der Tol, Mirco Migliavacca, and U. Rascher. 2018. "Remote Sensing of Plant-Water Relations: An Overview and Future Perspectives." *Journal of Plant Physiology* 227: 3–19.

Delalieux, Stephanie, Ben Somers, W. W. Verstraeten, J. A. N. Van Aardt, W. Keulemans, and Pol Coppin. 2009. "Hyperspectral Indices to Diagnose Leaf Biotic Stress of Apple Plants, Considering Leaf Phenology." *International Journal of Remote Sensing* 30 (8): 1887–1912.

DJI. 2019. "MATRICE 600 PRO SPECS." 2019. https://www.dji.com/matrice600-pro/info#specs.

"Finger Lakes Wine." 2017. 2017. https://www.wine-searcher.com/regions-finger+lakes.

Gago, J., C.B. Douthe, R. Coopman, P. Gallego, M. Ribas-Carbo, J. Flexas, J. Escalona, and H. Medrano. 2015. "UAVs Challenge to Assess Water Stress for Sustainable Agriculture." *Agricultural Water Management* 153: 9–19.

Gao, Bo-Cai, and Alexander FH Goetz. 1990. "Column Atmospheric Water Vapor and Vegetation Liquid Water Retrievals from Airborne Imaging Spectrometer Data." *Journal of*

Geophysical Research: Atmospheres 95 (D4): 3549–64.

Geladi, Paul, and Bruce R. Kowalski. 1986. “Partial Least-Squares Regression: A Tutorial.” *Analytica Chimica Acta* 185: 1–17.

“Geological Features of Fox Run Vineyards in the Finger Lakes.” 2019. 2019. https://foxrunvineyards.com/ourstory-geologicalfeatures.asp.

Govender, M., P. J. Govender, I. M. Weiersbye, E. T. F. Witkowski, and F. Ahmed. 2009. “Review of Commonly Used Remote Sensing and Ground-Based Technologies to Measure Plant Water Stress.” *Water* 35 (5).

Hall, Andrew, D. W. Lamb, Bruno Holzapfel, and J. Louis. 2002. “Optical Remote Sensing Applications in Viticulture-a Review.” *Australian Journal of Grape and Wine Research* 8 (1): 36–47.

Headwall. 2018. “Headwall Nano-Hyperspec® Hyperspectral Imaging Sensor Product Data Sheet.” 2018. https://cdn2.hubspot.net/hubfs/145999/June 2018 Collateral/NanoHyperspec0118.pdf.

“History of Fox Run.” 2019. 2019. https://foxrunvineyards.com/ourstory-history.asp.

Izzo, Rinaldo R., Alan N. Lakso, Evan D. Marcellus, Timothy D. Bauch, Nina G. Raqueño, and Jan van Aardt. 2019. “An Initial Analysis of Real-Time SUAS-Based Detection of Grapevine Water Status in the Finger Lakes Wine Country of Upstate New York.” In *Autonomous Air and Ground Sensing Systems for Agricultural Optimization and Phenotyping IV*, 1100811. International Society for Optics and Photonics.

Jin, Xiaoli, Chunhai Shi, Chang Yeon Yu, Toshihiko Yamada, and Erik J. Sacks. 2017. “Determination of Leaf Water Content by Visible and Near-Infrared Spectrometry and Multivariate Calibration in Miscanthus.” *Frontiers in Plant Science* 8: 721.

Jones, Hamlyn G., Rachid Serraj, Brian R. Loveys, Lizhong Xiong, Ashley Wheaton, and Adam H. Price. 2009. “Thermal Infrared Imaging of Crop Canopies for the Remote Diagnosis and Quantification of Plant Responses to Water Stress in the Field.” *Functional Plant Biology* 36 (11): 978–89.

Jones, Hamlyn G., Manfred Stoll, Tiago Santos, Claudia de Sousa, M. Manuela Chaves, and Olga M. Grant. 2002. “Use of Infrared Thermography for Monitoring Stomatal Closure in the Field: Application to Grapevine.” *Journal of Experimental Botany* 53 (378): 2249–60.

Kokaly, Raymond F., and Roger N. Clark. 1999. “Spectroscopic Determination of Leaf Biochemistry Using Band-Depth Analysis of Absorption Features and Stepwise Multiple Linear Regression.” *Remote Sensing of Environment* 67 (3): 267–87.

Kuching, Sarawak. 2007. “The Performance of Maximum Likelihood, Spectral Angle Mapper, Neural Network and Decision Tree Classifiers in Hyperspectral Image Analysis.” *Journal of Computer Science* 3 (6): 419–23.

Leeuwen, C. van, P. Pieri, and P. Vivin. 2010. *Methodologies and Results in Grapevine Research*. London & New York: Springer, Dordrecht, Heidelberg.

Leeuwen, Cornelis Van, and Gerard Seguin. 2006. “The Concept of Terroir in Viticulture.” *Journal of Wine Research* 17 (1): 1–10.

Leeuwen, Cornelis Van, Olivier Trégoat, Xavier Choné, Benjamin Bois, David Pernet, and Jean-Pierre Gaudillère. 2009. “Vine Water Status Is a Key Factor in Grape Ripening and Vintage Quality for Red Bordeaux Wine. How Can It Be Assessed for Vineyard Management Purposes?” *OENO One* 43 (3): 121–34.

Loggenberg, Kyle, Albert Strever, Berno Greyling, and Nitesh Poona. 2018. “Modelling Water Stress in a Shiraz Vineyard Using Hyperspectral Imaging and Machine Learning.” *Remote Sensing* 10 (2): 202.

Maimaitiyiming, Matthew, Abduwasit Ghulam, Arianna Bozzolo, Joseph L. Wilkins, and Misha T. Kwasniewski. 2017. “Early Detection of Plant Physiological Responses to Different Levels of Water Stress Using Reflectance Spectroscopy.” *Remote Sensing* 9 (7): 745.

Matthews, Mark A., and Michael M. Anderson. 1989. “Reproductive Development in Grape (Vitis Vinifera L.): Responses to Seasonal Water Deficits.” *American Journal of Enology and Viticulture* 40 (1): 52–60.

Mehmood, Tahir, Kristian Hovde Liland, Lars Snipen, and Solve Sæbø. 2012. “A Review of Variable Selection Methods in Partial Least Squares Regression.” *Chemometrics and Intelligent Laboratory Systems* 118: 62–69.

Möller, M., V. Alchanatis, Y. Cohen, M. Meron, J. Tsipris, A. Naor, V. Ostrovsky, M. Sprintsin, and S. Cohen. 2006. “Use of Thermal and Visible Imagery for Estimating Crop Water Status of Irrigated Grapevine.” *Journal of Experimental Botany* 58 (4): 827–38.

Mulla, David J. 2013. “Twenty Five Years of Remote Sensing in Precision Agriculture: Key Advances and Remaining Knowledge Gaps.” *Biosystems Engineering* 114 (4): 358–71.

Newman, James L. 1986. “Vines, Wines, and Regional Identity in the Finger Lakes Region.” *Geographical Review*, 301–16.

O’brien, Robert M. 2007. “A Caution Regarding Rules of Thumb for Variance Inflation Factors.” *Quality & Quantity* 41 (5): 673–90.

Ojeda, Hernán, Claude Andary, Elena Kraeva, Alain Carbonneau, and Alain Deloire. 2002. “Influence of Pre-and Postveraison Water Deficit on Synthesis and Concentration of Skin Phenolic Compounds during Berry Growth of Vitis Vinifera Cv. Shiraz.” *American Journal of Enology and Viticulture* 53 (4): 261–67.

Penuelas, J., F. Baret, and I. Filella. 1995. “Semi-Empirical Indices to Assess Carotenoids/Chlorophyll a Ratio from Leaf Spectral Reflectance.” *Photosynthetica* 31 (2): 221–30.

Peñuelas, J., J. Pinol, R. Ogaya, and I. Filella. 1997. “Estimation of Plant Water Concentration by the Reflectance Water Index WI (R900/R970).” *International Journal of Remote Sensing* 18 (13): 2869–75.

Peñuelas, Josep, and Iolanda Filella. 1998. “Visible and Near-Infrared Reflectance Techniques for Diagnosing Plant Physiological Status.” *Trends in Plant Science* 3 (4): 151–56.

Pôças, Isabel, Arlete Rodrigues, Sara Gonçalves, Patrícia Costa, Igor Gonçalves, Luís Pereira, and Mário Cunha. 2015. “Predicting Grapevine Water Status Based on Hyperspectral Reflectance Vegetation Indices.” *Remote Sensing* 7 (12): 16460–79.

Prasad, Kumar Arun, Lakshmanan Gnanappazham, Vaithilingam Selvam, Ramasamy Ramasubramanian, and Chandra Sekar Kar. 2015. “Developing a Spectral Library of Mangrove Species of Indian East Coast Using Field Spectroscopy.” *Geocarto International* 30 (5): 580–99.

Primicerio, Jacopo, Salvatore Filippo Di Gennaro, Edoardo Fiorillo, Lorenzo Genesio, Emanuele Lugato, Alessandro Matese, and Francesco Primo Vaccari. 2012. “A Flexible Unmanned Aerial Vehicle for Precision Agriculture.” *Precision Agriculture* 13 (4): 517–23.

Rapaport, Tal, Uri Hochberg, Maxim Shoshany, Arnon Karnieli, and Shimon Rachmilevitch. 2015. “Combining Leaf Physiology, Hyperspectral Imaging and Partial Least Squares-Regression (PLS-R) for Grapevine Water Status Assessment.” *ISPRS Journal of Photogrammetry and Remote Sensing* 109: 88–97.

Roberts, D. 1985. “Calibration of Airborne Imaging Spectrometer Data to Percent Reflectance Using Field Spectral Measurements.” In *International Symposium on Remote Sensing of Environment*, 679–88.

Rodríguez-Pérez, José R., David Riaño, Eli Carlisle, Susan Ustin, and David R. Smart. 2007. “Evaluation of Hyperspectral Reflectance Indexes to Detect Grapevine Water Status in Vineyards.” *American Journal of Enology and Viticulture 58* 58 (3): 302–17.

Santesteban, L. G., S. F. Di Gennaro, A. Herrero-Langreo, C. Miranda, J. B. Royo, and A. Matese. 2017. “High-Resolution UAV-Based Thermal Imaging to Estimate the Instantaneous and Seasonal Variability of Plant Water Status within a Vineyard.” *Agricultural Water Management* 183: 49–59.

Santos, Antonio Odair, and Oren Kaye. 2009. “Grapevine Leaf Water Potential Based upon near Infrared Spectroscopy.” *Scientia Agricola* 66 (3): 287–92.

Savitzky, Abraham, and Marcel JE Golay. 1964. “Smoothing and Differentiation of Data by Simplified Least Squares Procedures.” *Analytical Chemistry* 36 (8): 1627–39.

Schmidt, K. S., and A. K. Skidmore. 2004. “Smoothing Vegetation Spectra with Wavelets.” *International Journal of Remote Sensing* 25 (6): 1167–84.

Scholander, Per F., Edda D. Bradstreet, E. A. Hemmingsen, and H. T. Hammel. 1965. “Sap Pressure in Vascular Plants: Negative Hydrostatic Pressure Can Be Measured in Plants.” *Science* 148 (3668): 339–46.

“Scikit-Learn.” 2019. 2019. https://scikit-learn.org/stable/.

Serrano, Lydia, Cristina González-Flor, and Gil Gorchs. 2012. “Assessment of Grape Yield and Composition Using the Reflectance Based Water Index in Mediterranean Rainfed Vineyards.” *Remote Sensing of Environment* 118: 249–58.

Shapiro, Samuel Sanford, and Martin B. Wilk. 1965. “An Analysis of Variance Test for Normality (Complete Samples).” *Biometrika* 52 (3/4): 591–611.

Smith, Geoffrey M., and Edward J. Milton. 1999. “The Use of the Empirical Line Method to Calibrate Remotely Sensed Data to Reflectance.” *International Journal of Remote Sensing* 20 (13): 2653–62.

SPH. 2019. “UgCS.” 2019. https://www.ugcs.com/.

SVC. 2019. “HR-1024i.” 2019. https://www.spectravista.com/our-instruments/hr-1024i/.

Thenkabail, P.S., J.G. Lyon, and A. Huete. 2011. *Advances in Hyperspectral Remote Sensing of Vegetation and Agricultural Crops*. Florida, USA: CRC Press.

Tico, M., and M. Vehvilainen. 2006. “Estimation of Motion Blur Point Spread Function from Differently Exposed Image Frames.” In *IEEE 14th European Signal Processing Conference*, 1–4.

Trimble Navigation. 2017. “APX-15 UAV Data Sheet.” 2017. https://www.applanix.com/downloads/products/specs/APX15_UAV.pdf.

Turner, D., A. Lucieer, and C. Watson. 2011. “Development of an Unmanned Aerial Vehicle (UAV) for Hyper Resolution Vineyard Mapping Based on Visible, Multispectral, and Thermal Imagery.” In *34th International Symposium on Remote Sensing of Environment*, 4.

Turner, Neil C. 1988. “Measurement of Plant Water Status by the Pressure Chamber Technique.” *Irrigation Science* 9 (4): 289–308.

“Vineyard Map of Fox Run Vineyards.” 2019. 2019. https://foxrunvineyards.com/ourstory-vineyardmap.asp.

Wold, Svante, Michael Sjöström, and Lennart Eriksson. 2001. “PLS-Regression: A Basic Tool of Chemometrics.” *Chemometrics and Intelligent Laboratory Systems* 58 (2): 109–30.

Zarco-Tejada, Pablo J., Alberto Berjón, Raúl López-Lozano, John R. Miller, P. Martín, Victoria Cachorro, M. R. González, and A. De Frutos. 2005. “Assessing Vineyard Condition with Hyperspectral Indices: Leaf and Canopy Reflectance Simulation in a Row-Structured Discontinuous Canopy.” *Remote Sensing of Environment* 99 (3): 271–87.

Zarco-Tejada, Pablo J., Victoria González-Dugo, L. E. Williams, L. Suárez, José AJ Berni, D. Goldhamer, and E. Fereres. 2013. “A PRI-Based Water Stress Index Combining Structural and Chlorophyll Effects: Assessment Using Diurnal Narrow-Band Airborne Imagery and the CWSI Thermal Index.” *Remote Sensing of Environment* 138: 38–50.

Zovko, Monika, Uroš Žibrat, Matej Knapič, M. Bubalo Kovačić, and Davor Romić. 2019. “Hyperspectral Remote Sensing of Grapevine Drought Stress.” *Precision Agriculture* 20 (2): 335–47.